CHAPTER SEVEN

Electroporation of Planar Lipid Bilayers and Membranes

Mojca Pavlin, Tadej Kotnik, Damijan Miklavčič, Peter Kramar, *and*
Alenka Maček Lebar[1],[*]

Contents

[*] Corresponding author. Tel.: +386 1 4768 770; Fax: +386 1 4264 658
E-mail address: alenka.maceklebar@fe.uni-lj.si (A. Maček Lebar).

[1] University of Ljubljana, Faculty of Electrical Engineering, Tržaška 25, SI-1000 Ljubljana, Slovenia

Abstract

Strong external electric field can destabilize membranes and induce formation of pores thus increasing membrane permeability. The phenomenon is known as membrane electroporation, sometimes referred to also as dielectric breakdown or electropermeabilization. The structural changes involving rearrangement of the phospholipid bilayer presumably lead to the formation of aqueous pores, which increases the conductivity of the membrane and its permeability to water-soluble molecules which otherwise are deprived of membrane transport mechanisms. This was shown in variety of experimental conditions, on artificial membranes such as planar lipid bilayers and vesicles, as well as on biological cells *in vitro* and *in vivo*. While studies of electroporation on artificial lipid bilayers enabled characterization of the biophysical processes, electroporation of biological cells led to the development of numerous biomedical applications. Namely, cell electroporation increases membrane permeability to otherwise nonpermeant molecules, which allows different biological and medical applications including transfer of genes (electrogene transfer), transdermal drug delivery and electrochemotherapy of tumors. In general, the key parameter for electroporation is the induced transmembrane voltage generated by an external electric field due to the difference in the electric properties of the membrane and the external medium, known as Maxwell–Wagner polarization. It was also shown that pore formation and the effectiveness of cell electroporation depend on parameters of electric pulses like number, duration, repetition frequency and electric field strength, where the later is the crucial parameter since increased transmembrane transport due to electroporation is only observed above a certain threshold field. Two main theoretical approaches were developed to describe electroporation. The electromechanical approach considers membranes as elastic or viscoelastic bodies, and applying principles of electrostatics and elasticity predict membrane rupture above critical membrane voltage. A conceptually different approach describing formation and expansion of pores is based on energy consideration; it is assumed that external electric field reduces the free energy barrier for formation of hydrophilic pores due to lower polarization energy of water in the pores compared to the membrane. Combined with stochastic mechanism of pores expansion it can describe experimental data of bilayer membranes. Still, the molecular mechanisms of pore formation and stabilization during electroporation are not fully understood and rigorous experimental conformation of different theories is still lacking.

    The focus of this chapter is to review experimental and theoretical data in the field of electroporation and to connect biophysical aspects of the process with the phenomenological experimental observations obtained on planar lipid bilayers, vesicles and cells.

1. Introduction

Biological membranes play a crucial role in living organisms. They are soft condensed matter structures that envelope the cells and their inner organelles. Biological membranes maintain relevant concentration gradients by acting as selective filters toward ions and molecules. Besides their passive role, they also host a number of metabolic and biosynthetic activities [1].

The interaction of electric fields with biological membranes and pure phospholipid bilayers has been extensively studied in the last decades [2,3]. Strong external electric field can destabilizes membranes and induce changes in their structure. The key parameter is the induced-transmembrane voltage generated by an external electric field due to the difference in the electric properties of the membrane and the external medium, known as Maxwell–Wagner polarization. According to the most plausible theory until now the lipids in the membrane are rearranged to form aqueous pores which increases the conductivity of the membrane and its permeability to water-soluble molecules which otherwise are deprived of membrane transport mechanisms. Therefore this phenomenon is known as electroporation, sometimes referred to also as dielectric breakdown or electropermeabilization of membranes.

Reversible "electrical breakdown" of the membrane has first been reported by Stampfli in 1958 [4], but for some time this report has been mostly unnoticed. Nearly a decade later, Sale and Hamilton reported on nonthermal electrical destruction of microorganisms using strong electric pulses [5]. In 1972, Neumann and Rosenheck showed that electric pulses induce a large increase of membrane permeability in vesicles [6]. Following these pioneering studies three important works have motivated a series of further investigations. First, Neumann *et al.* showed in 1982 that genes can be transferred into the cells by using exponentially decaying electric pulses [7]. A few years later, in 1987, Okino and Mohri and, in 1988, Mir *et al.* showed that definite amounts of molecules are introduced into the cells in either *in vivo* or *in vitro* conditions, by using electric pulses [8,9]. Most of the early work was done on isolated cells in conditions *in vitro*, but it is now known that many applications are also successful in *in vivo* situation. It was showed that using electroporation, small and large molecules can be introduced into cells and extracted from cells, and proteins can be inserted into the membrane and cells can be fused. As a result of its efficiency, electroporation has rapidly found its applications in many fields of biochemistry, molecular biology and medicine.

By applying an electric field of adequate strength and duration, the membrane returns into its normal state after the end of the exposure to the electric field – electroporation is reversible. However, if the exposure to electric field is too long or the strength of the electric field is too high, the membrane does not reseal after the end of the exposure, and electroporation is irreversible in such a case. According to the type of electroporation (i.e. reversible or irreversible), two groups of applications exist: functional, where functionality of cells, tissues or microorganisms must be sustained; and destructive, where electric fields are used to destroy plasma membranes of cells or microorganisms [10].

Irreversible electroporation can be used for nonthermal food and water preservation, where permanent destruction of microorganisms is required [11–13].

Functional applications are currently more widespread and established in different experimental or practical protocols. Probably, the most important functional application is the introduction of a definite amount of small or large molecules to the cytoplasm through the plasma membrane [14,15]. Electrochemotherapy (ECT) is a therapeutic approach in cancer treatment that combines chemotherapy and electroporation. The delivery of electric pulses at the time when a chemotherapeutic drug reaches its highest extracellular concentration considerably increases the transport through the membrane toward the intracellular targets and cytotoxicity of a drug is enhanced. In several preclinical and clinical studies, either on humans or animals, it was demonstrated that ECT can be used as the treatment of choice in local cancer treatment [16–18]. Application of electroporation for transfer of DNA molecules into the cell is referred to as electrogenetransfection (EGT) and has not yet entered clinical trials [15]. Another application of electroporation is insertion of molecules into the cell membrane. As the membrane reseals, it entraps some of the transported molecules, and if these molecules are amphipathic (constituted of both polar and nonpolar regions), they can remain stably incorporated in the membrane [19,20]. Under appropriate experimental conditions, delivery of electric pulses can lead to the fusion of membranes of adjacent cells. Electrofusion has been observed between suspended cells [21,22], and even between cells in tissue [23]. For successful electrofusion in suspension, the cells must previously be brought into close contact, for example, by dielectrophoresis [21]. Electrofusion has proved to be a successful approach in production of vaccines [24] and antibodies [25].

Application of high-voltage pulses to the skin causes a large increase in ionic and molecular transport across the skin [26]. This has been applied for transdermal delivery of drugs [27] and also works for larger molecules, for example, DNA oligonucleotides [28].

In spite of successful use of electroporation in biomedical applications, the molecular mechanisms of the involved processes are still not fully explained and there is lack of connection between experimental data and theoretical descriptions of pore formation [2,29–32]. It was shown that pore formation and the effectiveness of cell electroporation depend on parameters of electric pulses like number (N), duration (T), repetition frequency (f) and electric field strength (E). The later is the crucial parameter since increased transmembrane transport due to electroporation is only observed above a certain threshold field. It was also shown [33,34] that neither electrical energy nor charge of the electric pulses alone determine the extent of electroporation consequences and that the dependency on E, N and T is more complex [35].

Electroporation has been observed and studied in many different systems, i.e. artificial planar lipid bilayers, giant lipid vesicles, cells *in vitro* and *in vivo*. Cell membranes are much more complicated than artificial lipid structures, with respect to geometry, composition and the presence of active processes. The problem associated with the complexity of natural cell membranes can be avoided by investigating synthetic liposomes or vesicles which mimic the geometry and the size of cell membranes, but are void of ion channels and the multitude of other embedded

components. Artificial planar lipid bilayer is the simpliest modeling lipid system that also has the geometric advantage of providing electrical and chemical access to both sides of a membrane.

In the following, we shall review experimental and theoretical data in the field of electroporation and connect biophysical aspects of the process with the phenomenological experimental observations obtained on planar lipid bilayers, vesicles and cells.

2. EXPERIMENTAL INVESTIGATION OF ELECTROPORATION ON PLANAR LIPID BILAYERS

The planar lipid bilayer can be considered as a small fraction of total cell membrane. As such has often been used to investigate basic aspects of electroporation; especially because of its geometric advantage of allowing chemical and electrical access to both sides of a membrane. Planar lipid bilayers can generally be formed by three different techniques: painting technique, folding technique or tip-dip technique [36]. In either case a thin bi-molecular film composed of specified phospholipids and organic solvent is formed on a small aperture in a hydrophobic partition separating two aqueous compartments. Electrodes plunged in the aqueous compartments permit the measurement of currents and voltages across the membrane. By reason of that two measuring principles of planar lipid bilayer's properties are commonly used (Fig. 1): voltage clamp method [37–48] and current clamp method [49,50,51–59]. From an electrical point of view a planar lipid bilayer can be regarded as a nonconducting capacitor, therefore two electrical properties, capacitance (C) and resistance (R), mostly determine its behavior.

When voltage clamp method is used the voltage signal is applied to the planar lipid bilayer; either a step change [47], pulse [37,41,44], linear rising [60] or some other shape of the voltage signal. The simplest as well as mostly used shape of the voltage signal is a square voltage pulse [37,41]. It is commonly used for
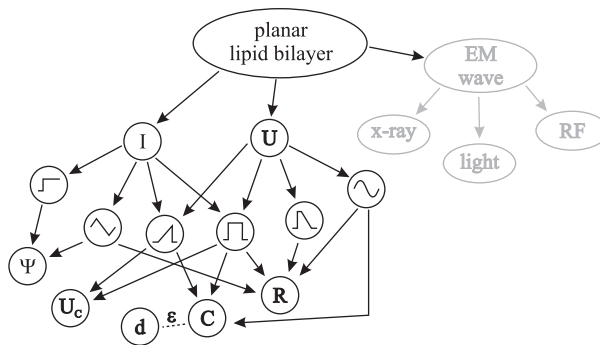
Figure 1 Electrical properties of planar lipid bilayer: resistance (R), capacitance (C), thickness (d), voltage breakdown (U_c) and mass fluctuation (Ψ) are measured with application of current (I) or voltage (U).

determination of planar lipid bilayer breakdown voltage (U_c) and capacitance [44]. Some experiments were done by two sinus-shaped voltage signals: the first with low frequency and large amplitude and the second with high frequency and low amplitude that was added to the first one. In this way lipid bilayer conductance and capacitance were determined at the same time [59]. When current clamp method is used, the current is applied to the lipid bilayer. Usually this method is appropriate for measuring resistance of a planar lipid bilayer and mass flow through it as a consequence of increased membrane permeability. It is believed that during this kind of measurements the lipid bilayer is more stable due to less voltage stress [50,53]; therefore, also small changes in membrane structure and the occurrence of fluctuating defects can be observed [45,50,54]. Scalas *et al.* [54], for example, reported on time course of voltage fluctuations that followed an increase of the membrane conductance due to the opening and closing hydrophilic pores.

Combination of electrical recording techniques with different kinds of high frequency electromagnetic fields offers additional investigations of structure–function relationships of planar lipid bilayer and of membrane interacting peptides [61–64]. For structure elucidation of lipid–water mesophases, small- and wide-angle X-ray scattering method were used [61]. Hanyu *et al.* [62] have presented an experimental system which allows measurement of current (function) and fluorescence emission (structural change) of an ion channel in planar lipid bilayer while membrane potential is controlled [62]. Rapid and reversible changes in photo responsive planar lipid bilayers electrical properties when irradiated with light were studied by Yamaguchi *et al.* [63]. Planar lipid bilayers have been also exposed to RF-field of about 900 MHz according to GSM standards and authors have revealed that temperature oscillations due to the pulsed radio frequency fields are too small to influence planar lipid bilayer's low frequency behavior [64].

2.1. Breakdown Voltage

Breakdown voltage (U_c) is one of the most important properties of a lipid bilayer when biomedical and biotechnological applications of electroporation are under consideration. It has been measured either by voltage clamp or current clamp method using rectangular, triangular or step shape of the signal (Fig. 1). Mostly, the breakdown voltage of the planar lipid bilayer is determined by a rectangular voltage pulse (10 µs–10 s). The amplitude of the voltage pulse is incremented in small steps until the breakdown of the bilayer is obtained [37]. First the voltage pulse charges up the planar lipid bilayer. Above a critical voltage (breakdown voltage U_c) defects are created in the planar lipid bilayer allowing an increase of the transmembrane current. Usually membrane collapses then after.

The influence of various factors, such as lipid composition [37,38,55], organic solvent [41], temperature [44] and electrolyte composition [43,44], on the absolute value of U_c has been studied. Benz *et al.* have measured U_c by presence of various salts in the electrolyte bathing the membranes [44] and shown that presence of Li^+, Na^+, K^+, Rb^+ or Cs^+ ions do not change U_c. It was also proved that ionic strength of bathing solution had no influence on U_c [40,43]. Experiments have demonstrated that with increasing temperature U_c of planar lipid bilayer decrease. [44].

Table 1 U_c of planar lipid bilayer composed if lipid molecules of a single type. All measurements have been done using 0.1 M KCl as a bathing solution.

BLM	U_c (mV)	Method	Reference
Azolecitin	423	Voltage clamp – 100 µs pulse	[38]
POPC	450	Voltage clamp – 100 µs pulse	[37,39,40]
POPS	480	Voltage clamp – 100 µs pulse	[39,40]
Egg PC	280	Current clamp – triangle (1.6–2.5 mHz)	[52,55]
DPh PC	390	Current clamp – triangle (1.6–2.5 mHz)	[52,55]
	527	Voltage clamp – 10 µs pulse	[39,40]
DPh PS	525	Voltage clamp – 10 µs pulse	[39,40]
PS	500	Current clamp – triangle (2.5 mHz)	[55]
GM	170	Current clamp – triangle (2.5 mHz)	[55]

Table 2 U_c of planar lipid bilayer composed from two lipid molecules or lipid molecules and surfactants. All measurements have been done using 0.1 M KCl as a bathing solution.

BLM	U_c (mV)	Method	Reference
Azolecitin+Poloxamer 188	448	Voltage clamp – 10 µs pulse	[38]
POPC+0.1 µM $C_{12}E_8$	383	Voltage clamp – 10 µs pulse	[37]
POPC+1 µM $C_{12}E_8$	333	Voltage clamp – 10 µs pulse	[37]
POPC+10 µM $C_{12}E_8$	333	Voltage clamp – 10 µs pulse	[37]
Egg PC/Ch 4:1	270	Current clamp – triangle (2.5 mHz)	[55]

U_c depends on a type of hydrophilic chain of the lipids (Table 1). Meier has reported that palmitoyl-oleoyl (PO) membrane require ∼100 mV smaller breakdown voltages compared to diphytanoyl (DPh) membranes [39].

Incorporation of nonphospholipid substances into planar lipid bilayer changes the intensity and duration of the electrical stimulus needed for breakdown. Such effect is a consequence of the surfactant molecular shape acting to change the spontaneous curvature of the membrane, which is especially important during the defects formation process. Troiano *et al.* [37] performed a quantitative study on the effect of $C_{12}E_8$ on planar lipid bilayer made of 1-palmitoyl 2-oleoyl phosphatidylcholine (POPC). Their results and results of some other studies are gathered in Table 2.

Using voltage pulse protocol the number of applied voltage pulses is not known in advance and each bilayer is exposed to voltage stress many times. Such a pretreatment of the lipid bilayer affects its stability and consequently the determined breakdown voltage of the lipid bilayer [47]. Another approach for the breakdown voltage determination was suggested by our group [60]. Using linear rising signal the breakdown voltage is determined by a single voltage exposure.

Our system for following up electroporation of planar lipid bilayers consists of a signal generator, a Teflon chamber and a device, which is used for measurements of membrane current and voltage (Fig. 2).
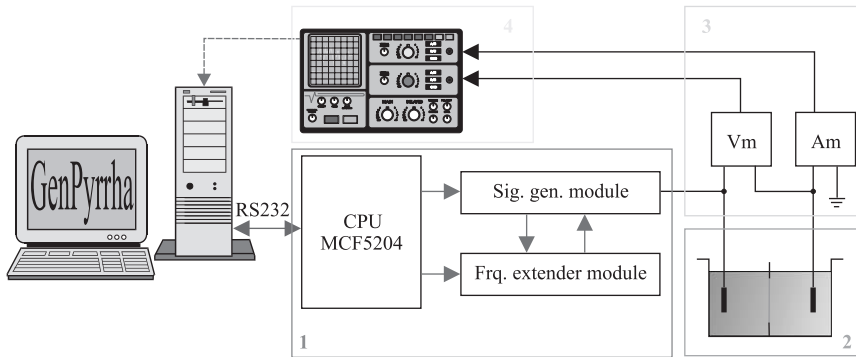
Figure 2 System for electroporation of planar lipid bilayer. (1) The microprocessor board with MCF5204 processor and two modules. One module generates arbitrary signals and the other that is realized in Xillinx, is used for frequency extension. (2) Chamber for forming lipid bilayers and two Ag–AgCl electrodes. (3) Modules for current and voltage amplification. (4) Digital oscilloscope for data storing [60].

Signal generator is a voltage generator of an arbitrary type that provides voltage amplitudes from −5 to +5 V. It is controlled by costume written software (Genpyrrha), specially designed for drawing the voltage signal that is used for membrane electroporation.

Two Ag–AgCl electrodes, one on each side of the planar lipid bilayer are plunged into the salt solution. Transmembrane voltage is measured via a LeCroy differential amplifier 1822. The same electrodes are used to measure transmembrane current. Both signals are stored in oscilloscope LeCroy Waverunner-2 354 M in Matlab format and processed offline.

Chamber is made out of Teflon. It consists of two cubed reservoirs with volume of 5.3 cm^3 each. In the hole between two reservoirs a thin Teflon sheet with a round hole (105 µm diameter) is inserted. Lipid bilayer is formed by the folding method [36,65].

Measurement protocol consists of two parts: capacitance measurement (Fig. 3A) and lipid bilayer breakdown voltage measurement (Fig. 3B). Capacitance of each planar lipid bilayer is measured by discharge method [60].

Breakdown voltage (U_c) of the lipid bilayer is measured then after by the linear rising signal. The slope of the linear rising signal (k) and the peak voltage of the signal have to be selected in advance. Breakdown voltage is defined as the voltage at the moment t_{br} when sudden increase of transmembrane current is observed. Time of breakdown t_{br} was defined as a lifetime of the lipid bilayer at a chosen slope of the linear rising signal (Fig. 3). Owing to already known experimental evidence that lipid bilayer lifetime is dependent on the applied voltage [37,66] and that the lipid bilayer breakdown voltage is dependent on the lipid bilayer pre-treatment [47], U_c and t_{br} are measured at six or seven different slopes. Indeed lifetime of lipid bilayer depends on the slope of linear rising voltage signal and also the breakdown voltage is a function of the slope of the linear rising voltage signal; it increases with increasing slope. Therefore, using nonlinear regression, *a* two parameters curve is
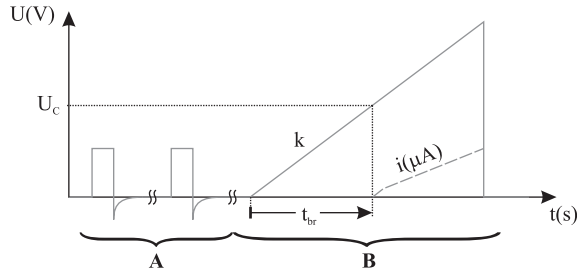
Figure 3 Measurement protocol: (A) capacitance measurement of lipid bilayer was measured in two steps. In the first step, we measured capacitance of the electronic system without lipid bilayer. Second step was measuring capacitance of electronic system with lipid bilayer and salt solution. (B) Voltage breakdown measurement with linear rising signal [60].

fitted to the data

$$U = \frac{a}{1 - e^{-t/b}} \qquad (1)$$

where U is U_c measured at different slopes, t the corresponding t_{br}, and a and b the parameters. Parameter a is an asymptote of the curve which corresponds to minimal breakdown voltage U_{cMIN} for specific bilayer. Parameter b governs the inclination of the curve.

The results obtained with described measuring protocol are presented in Fig. 4. U_c and t_{br} of POPC, POPC+1 μM $C_{12}E_8$ and palmitoyl-oleoyl phosphatidylserine (POPS):POPC (3:7) planar lipid bilayers have been measured and U_{cMIN} for each bilayer has been calculated. Computed parameter that corresponds to U_{cMIN} for specific bilayer is 0.49, 0.58 and 0.55 V, respectively.

Evans *et al.* used similar approach in their experiments on lipid vesicles [67]. They applied tension at different loading rates and they found out that tension needed for membrane rupture increases with increasing loading rate. As in our case the loading rate dependence of rupture events implies a kinetic process of defect formation (see theoretical explanations in the next chapter). It has to be noted that measuring protocol mentioned offers also better reproducibility and lower scattering of measured data due to the fact that each bilayer is exposed to electroporation treatment only once.

2.2. Capacitance

The capacitance (C) is a parameter that is considered to be the best tool for probing the stability and formal goodness of the planar lipid bilayer. It can be determined by various methods. Most common and simple method for measuring planar lipid bilayer capacitance is discharge pulse [38,41]. Galluci *et al.* have described a measurement system where two sinus signals with frequencies 1 Hz and 1 kHz are mixed and applied to planar lipid bilayer. Amplitude and phase of both signals governs planar lipid bilayer's capacitance and resistance simultaneously [68]. Such continuous monitoring of C may prove useful in tracking planar lipid bilayer electrical properties that depend on the lipids composition and incorporated
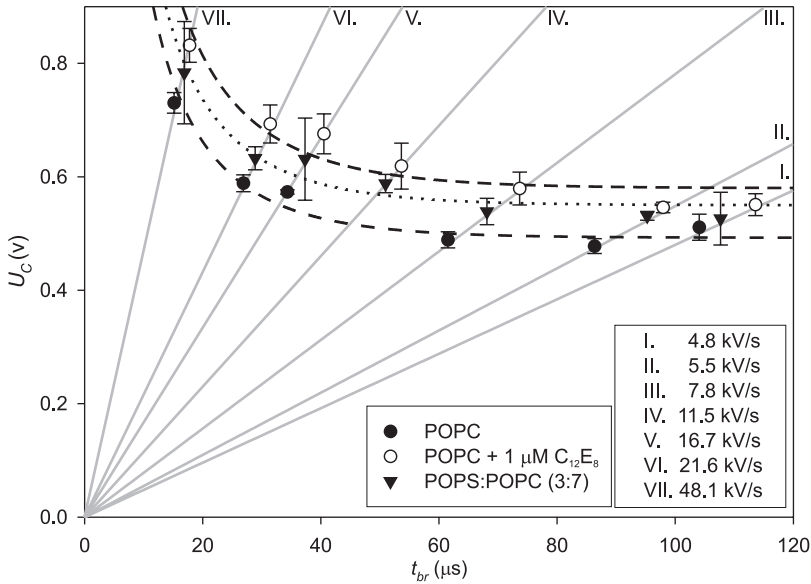
Figure 4   The breakdown voltage (U_c) (dots) of lipid bilayers as a function of lifetime t_{br}. The gray lines show seven different slopes (k) of applied liner rising voltage signal. Dash, dotted and dash–dotted curves represent two parameters curve fitted to data (1). Asymptotes of the curves (a) correspond to minimal breakdown voltage U_{cMIN} for lipid bilayers made of POPC, POPC+1 µM $C_{12}E_8$ and POPS:POPC (3:7) (Table 3).

nonphospholipids substances. Capacitance of planar lipid bilayer can also be determined by triangular voltage signal [49], that is controlled by the regulation system including charged planar lipid bilayer as a part. Therefore the period of the triangular voltage signal is related to capacitance of planar lipid bilayer. When current clamp method is used, capacitance of planar lipid bilayer can be measured with ramp signal [52,53,69].

Gallucci *et al.* have observed that the capacitance of planar lipid bilayer is dependent of concentration of salt solution. Capacitance measured in higher concentration of salt solution is lower than in lower concentration of salt solution [68]. Capacitances of planar lipid bilayers measured by various methods in different salt solutions are gathered in Table 3.

2.3. Conductance/Resistance

Resistance (R) or conductance (G) as electrical property of nonpermeablized planar lipid bilayer can be measured only during application of voltage or current signal. Galluci *et al.* [68] have developed the system for measuring G and C simultaneously and continuously as a function of time. This method allows measuring of electrical properties of nonpermeabilized planar lipid bilayer as well as during the process of defect formation and electroporation.

Melikov *et al.* [45] monitored fluctuations in planar lipid bilayer conductance induced by applying a voltage step of sufficiently high amplitude. They showed that

Table 3   Capacitance of planar lipid bilayers measured by various methods in dierent salt solutions.

BLM	C (μF/cm^2)	Salt solution	Method	Reference
Azolecitin	0.59	0.1 M KCl	Discharge pulse	[38]
	0.3–0.4	–	Current ramp	[69]
DOPC		0.1 M NaCl	Discharge pulse	[41]
DOPE		0.1 M NaCl	Discharge pulse	[41]
DPh PC	0.60–0.75	0.1 M KCl		[51–53,55]
	0.76–1.13	1 M KCl		[51,54]
	0.36	1 M NaCl	Discharge pulse	[41]
Ox Ch	0.555	1 M KCl	Discharge pulse	[41]
	0.5		Current ramp	[69]
	0.41	1 M KCl	Muxd sin wave	[59]
	0.45	0.1 M KCl	Muxd sin wave	[68]
	0.47	0.5 M KCl	Muxd sin wave	[68]
	0.40	1 M KCl	Muxd sin wave	[68]
PC	0.75	0.1 M KCl	Current clamp triangular	[52,55]
PI	0.25	1 M KCl	Muxd sin wave	[59]
	0.30	0.1 M KCl	Muxd sin wave	[68]
	0.27	0.5 M KCl	Muxd sin wave	[68]
	0.25	1 M KCl	Muxd sin wave	[68]
POPC	0.59	0.1 M KCl	Discharge pulse	[37]

the amplitude of fluctuations varied in a rather broad interval (form 150 to 1500 pS) and they related them with the formation of local conductive defects (see theoretical explanations in the next chapter).

Robello *et al*. [52] observed a sharp increase in conductance induced by external electric field obtained under current clamp conditions. They related it with creation of hydrophilic paths that increase the planar lipid bilayer conductance by one order of magnitude.

Similarly Kalinowski *et al*. [70] presented chronopotentiometric method for following planar lipid bilayer conductance during local conductive defects creation that also allows observing of their dynamical behavior. The voltage fluctuations reported in their work are consistent with theoretical models that predict formation of temporary aqueous pathways across the membrane.

3. ATTEMPTS OF THEORETICAL EXPLANATION OF ELECTROPORATION

A number of theoretical models have been put forward as possible explanations of electroporation. Here, an attempt will be made to present these models roughly in their chronological order of appearance, and to review them critically,

Table 4 Values of the quantities used in the evaluation of the models.

Parameter	Notation	Value	Reference or explanation
Membrane			
Electric conductivity	σ_m	$\sim 3 \times 10^{-7}$ S/m	[71]
Dielectric permittivity	ε_m	4.4×10^{-11} F/m	[71]
Elasticity module	Y	$\sim 1 \times 10^{8}$ N/m^2	[72]
Viscosity	μ	0.6 Ns/m^2	[73]
Surface tension	Γ	$\sim 1 \times 10^{-3}$ J/m^2	[32]
Edge tension	γ	$\sim 1 \times 10^{-11}$ J/m	[32]
Thickness (undistorted)	d_0	5×10^{-9} m	[1]
Cytoplasm			
Electric conductivity	σ_i	0.3 S/m	[74,75]
Dielectric permittivity	ε_i	7.1×10^{-10} F/m	Set at the same value as ε_e
Extracellular medium			
Electric conductivity	σ_e	1.2 S/m	[76] (blood serum at 35°C)
Dielectric permittivity	ε_e	7.1×10^{-10} F/m	[77] (physiological saline at 35°C)

comparing their properties and abilities to those that the complete theoretical description of electroporation should provide:

- A physically realistic picture of both the nonpermeabilized and the permeabilized membrane. Unlike a true breakdown process, electroporation does not lead to a total disintegration of the system, but is localized and often even reversible.
- Limited reversibility. Based on the amplitude and duration of electric pulses, the permeabilized state is either reversible or irreversible.
- Dependence on pulse duration and the number of pulses. With longer pulses, a lower amplitude suffices for achieving the permeabilized state.
- A realistic value of the minimal transmembrane voltage ("critical voltage") at which permeabilization occurs. Most of the presented models provide an expression for this voltage, typically a function of several quantities. By inserting the typical values of these quantities into the expressions, we assess their agreement with experimentally measured critical voltage, which is in the range of a few hundred millivolts. These values are given in Table 4, where those which are either known only up to an order of magnitude, or can vary considerably, are marked by a tilde.
- Stochasticity. Variability of the critical pulse amplitude in experiments on cells can largely be attributed to the variability of cell size within the treated population. However, a certain degree of stochasticity is also observed in electropermeabilization of pure lipid vesicles and planar bilayers. Some authors view the ability of a model to account for this as crucial [32].

$U = 0; \ d = d_0; \ S = S_0; \ V = V_0$

$U = 0.90\,U_c;$
$d \approx 0.73\,d_0;$
$S \approx 1.37\,S_0;$
$V = V_0$
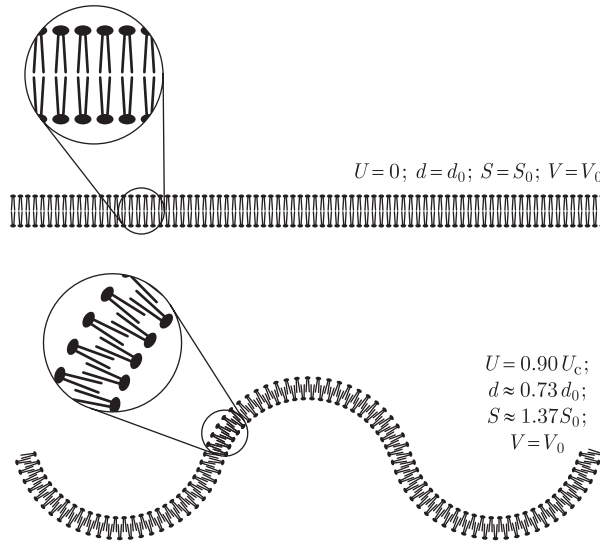
Figure 5 Membrane deformation according to the hydrodynamic model.

3.1. The Hydrodynamic Model

The hydrodynamic model, developed in the early 1970s [78,79], describes the membrane as a charged layer of a nonconductive and noncompressible liquid separating two conductive liquids. The transmembrane voltage exerts a pressure on this layer, and as it is assumed noncompressible in volume, the decrease in its thickness leads to an increase in its surface area. If either the volume enveloped by the membrane (in vesicles) or the perimeter of the membrane (in planar bilayers) is assumed to remain constant, the membrane thus becomes rippled (Fig. 5).

As the membrane surface area increases, so does its surface tension and thereby the pressure opposing the compression. At sufficiently low voltages, the two pressures reach an equilibrium at which the membrane thickness stabilizes. However, as shown in Appendix A.1, this equilibration is only possible up to the critical voltage given by

$$U_c = \sqrt{\frac{\Gamma d_0}{2\varepsilon_m}} \tag{2}$$

where Γ is the surface tension of the membrane, d_0 its uncompressed thickness and ε_m its dielectric permittivity. Above U_c an instability occurs: the compressive pressure prevails, causing a breakdown of the membrane. Applying typical parameter values from Table 4 to the above expression, we get $U_c \approx 0.24\,V$, which is in good agreement with the experimental data. The equations in Appendix A.1 also describe the membrane thickness as a function of the transmembrane voltage (Fig. 6).

The hydrodynamic model has several shortcomings. First, it applies to liquids with isotropic fluidity, which is not true for lipid bilayers, where transverse movement of molecules is very restricted. Second, it fails at the very first requirement listed at the beginning of this chapter, as it does not describe the permeabilized
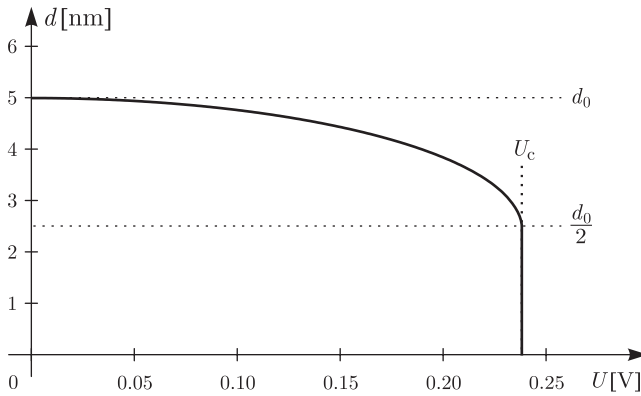
Figure 6 Membrane thickness as a function of the transmembrane voltage in the hydrodynamic model, using parameter values from Table 4.
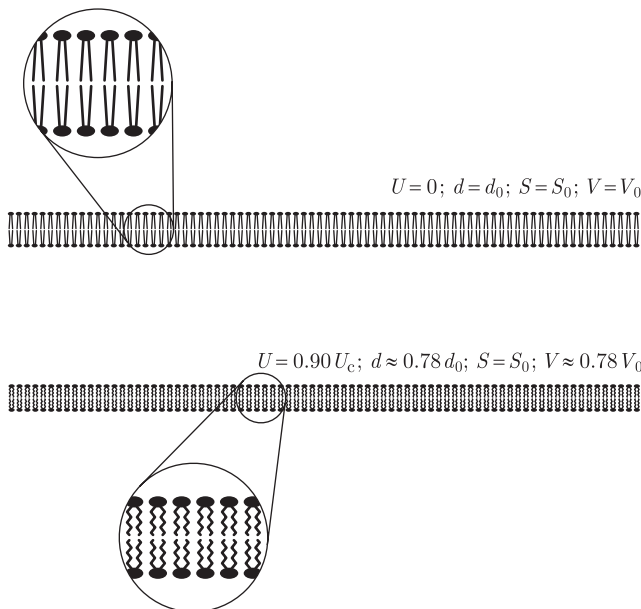
Figure 7 Membrane deformation according to the elastic model.

membrane. Of the other requirements, only the prediction of a realistic critical transmembrane voltage is met.

3.2. The Elastic Model

In contrast to the hydrodynamic model, which assumes a membrane with a constant volume and a variable surface, the elastic model, presented soon afterwards [80], assumes a variable volume and a constant surface (Fig. 7). In the elastic model,
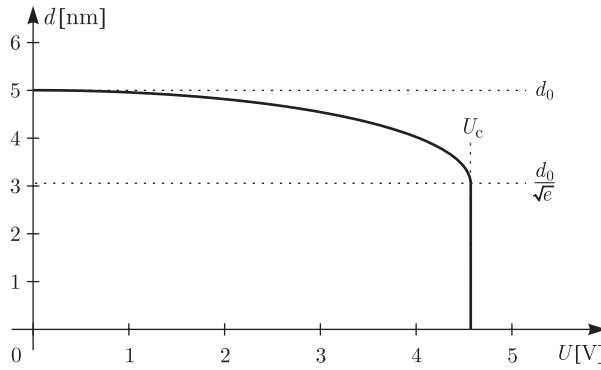
Figure 8 Membrane thickness as a function of the transmembrane voltage in the elastic model, using parameter values from Table 4.

the pressure exerted by the transmembrane voltage leads to a decrease in the volume of the membrane and an increase of elastic pressure opposing the compression. Also here, the equilibrium becomes impossible above a critical voltage (see Appendix A.2) given by

$$U_c \approx 0.61 \, d_0 \sqrt{\frac{Y}{\varepsilon_m}} \tag{3}$$

where Y is the elasticity module of the membrane, d_0 its uncompressed thickness and ε_m its dielectric permittivity. Above U_c, there is an instability similar to the one in the hydrodynamic model.

Applying typical parameter values (Table 4) to the expression above, we get $U_c \approx 4.57$ V, which is roughly an order of magnitude too large. With the equations in Appendix A.2, we can also plot the membrane thickness as a function of the transmembrane voltage (Fig. 8).

In addition to the unrealistic prediction of critical voltage, the model assumes that Y does not vary with deformation, which is certainly false at 39% compression of the membrane at the point of instability (Fig. 8). This model also offers no description of the permeabilized membrane, and fails to meet any other requirement listed at the beginning of this chapter.

3.3. The Hydroelastic Model

The assumptions on which the hydrodynamic and the elastic model are built are mutually excluding as well as unrealistic. By treating the membrane as a liquid with both surface tension and elasticity, one obtains the more realistic hydroelastic model, in which both the volume and the surface of the membrane vary, and the charged membrane both compresses in volume and forms ripples (Fig. 9).

Similarly to the two models described previously, the hydroelastic model predicts a compressive instability (see Appendix A.3). With typical parameter values (Table 4) it yields $U_c \approx 0.34$ V, which is in good agreement with experimental data.
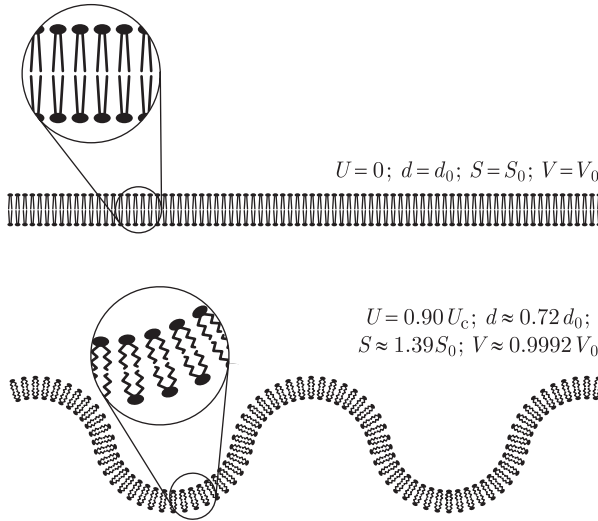
Figure 9   Membrane deformation according to the hydroelastic model.
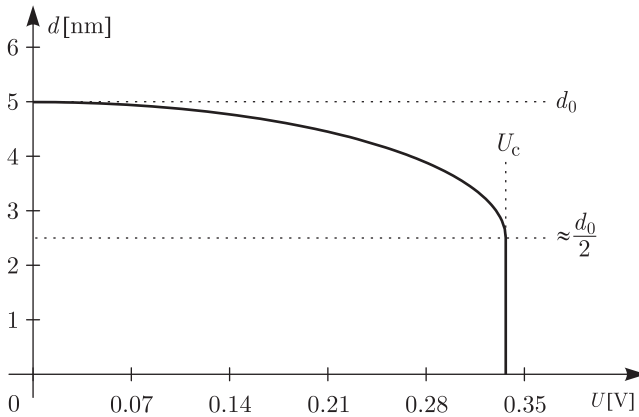
Figure 10   Membrane thickness as a function of the transmembrane voltage in the hydroelastic model, using parameter values from Table 4.

According to the hydroelastic model, at U_c the membrane thickness is reduced to 50% of the initial value (Fig. 10), its surface is enlarged to almost 200% of the initial value (Fig. 11) and the volume is reduced to 99.8% of the initial value (Fig. 12).

As Fig. 12 shows, according to the hydroelastic model the volume compression is very small, and even at the critical voltage the membrane volume is reduced by only 0.2% with respect to the initial value. Therefore, in this model the assumption of constant value of the elasticity module is much more reasonable than in the elastic model, in which the membrane breakdown is associated with a volume reduction of almost 39%. While the description of the compressive instability provided by the hydroelastic model is more realistic than those of the hydrodynamic
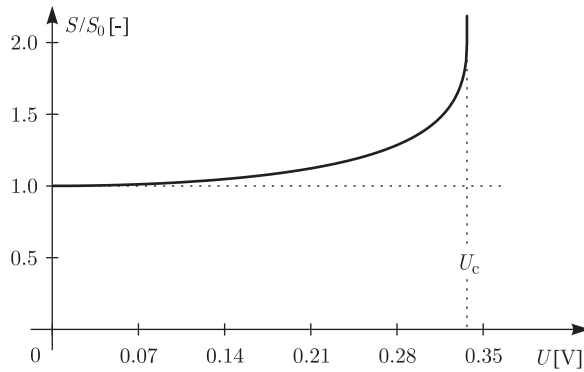
Figure 11 Membrane surface area as a function of the transmembrane voltage in the hydroelastic model, using parameter values from Table 4.
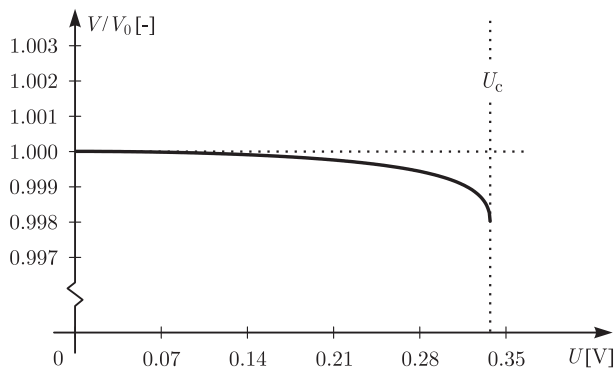
Figure 12 Membrane volume as a function of the transmembrane voltage in the hydroelastic model, using parameter values from Table 4.

and the elastic model, it has the same general drawback – it gives a nonsensical picture of the electropermabilized membrane: a uniform, infinitely thin layer, only this time a rippled one. With the exception of a realistic prediction of the critical transmembrane voltage, the model also fails to meet any other requirement given in the list at the beginning of this chapter.

3.4. The Viscohydroelastic Model

Making another step toward complexity, the viscohydroelastic model (referred to by its authors as viscoelastic) expands the hydroelastic model by adding to it the membrane viscosity [81,82]. As in the hydroelastic model, in this model the charged membrane is both compressed and rippled. However, the viscosity impedes the molecular flow, and thus the compression is not instantaneous, but follows the onset of the transmembrane voltage gradually.

During the compression and rippling of the membrane, the impeded molecular flow leads to the thinning of the membrane at those locations where the flow would
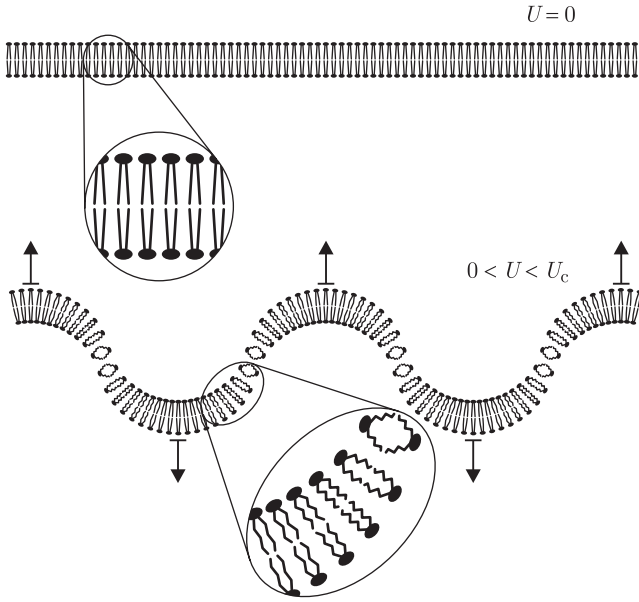
Figure 13   Membrane deformation according to the viscohydroelastic model.

have to be the most rapid to maintain the uniform thickness (Fig. 13). Up to a certain voltage, the membrane still reaches a state of equilibrium, but at higher voltages, the integrity of the membrane cannot be sustained and discontinuities form at the locations of the highest thinning. The analysis of such instability is elaborate and is described in more detail elsewhere [73,83], while Appendix A.4 gives a short outline of its results. This analysis shows that in the viscohydroelastic model, the instability occurs if the transmembrane voltage exceeds the critical amplitude given by

$$U_c = \sqrt[4]{\frac{8\,\Gamma Y d_0^3}{\varepsilon_m^2}} \qquad (4)$$

and lasts longer than the critical duration,

$$\tau_c = \frac{24\mu}{\frac{\varepsilon_m^2 U^4}{\Gamma d_0^3} - 8Y} \qquad (5)$$

where μ is membrane viscosity, the rest of the notation being the same as in the previously described models. Applying typical parameter values (Table 4), we get $U_c \approx 2.68$ V, so in this aspect the viscohydroelastic model performs worse than both the hydroelastic and the hydrodynamic model. However, it also offers a principal advantage over any of the previously described models, as the requirement of an above-critical voltage is linked to that of above-critical duration, providing a possible explanation of the dependence of permeabilization on the duration of electric
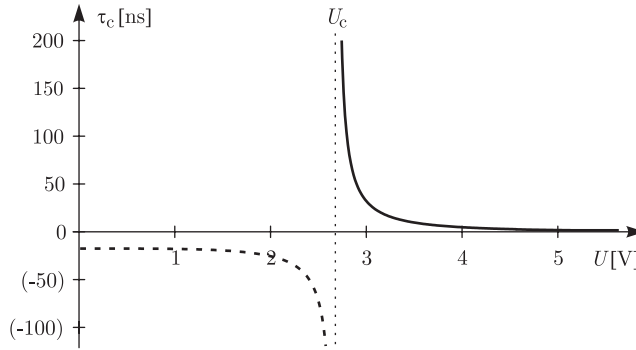
Figure 14   Critical duration of the transmembrane voltage as a function of its amplitude in the viscohydroelastic model, using parameter values from Table 4.

pulses. This is elucidated by Fig. 14, which shows the relation between the amplitude and the critical duration of the transmembrane voltage. At $U = 1.01 \times U_c \approx 2.71\,\mathrm{V}$, the critical duration τ_c of the transmembrane voltage is approximately 450 ns, which is in close agreement with the sub-microsecond imaging experiments [84,85]. Still, the critical duration in the model decreases extremely rapidly, and at $U = 1.20 \times U_c \approx 3.12\,\mathrm{V}$ we already have $\tau_c \approx 17\,\mathrm{ns}$, while experimentally this decrease is much slower. Also, according to the viscohydroelastic model, the permeabilized membrane is torn along the ripples, but no such disconnections have so far been observed, making this description of the permeabilized membrane questionable.

3.5. The Phase Transition Model

According to the models presented up to this point, electropermeabilization is a modification of the supramolecular membrane structure. In contrast, the phase transition model describes this phenomenon as a conformational change of membrane molecules [72]. On the molecular scale, the pressures are replaced by molecular energies, and the pressure equilibrium corresponds to the state of minimum free energy. With several minima of free energy, several stable states are possible, each corresponding to a distinct phase. In lipid bilayers, there are in general two such phases, solid (gel) and liquid phase.

The phase transition model of electropermeabilization is an extension of the statistical mechanical model of lipid membrane structure [86,87]. According to this model, the free energy of the membrane at a temperature T and an average molecular surface area S is given by an expression of a general form

$$W(T, S) = W_f(S) + W_c(T, S) + W_{ic}(T, S) + W_{ih}(T, S) \qquad (6)$$

where W_f is the flexibility energy (from continuous deformations, e.g. compression), W_c is the conformational energy (from discrete deformations, e.g. *trans–cis* transitions), W_{ic} is the energy of interactions between the hydrocarbon chains and W_{ih} is the energy of interactions between the polar heads of the lipids. Regrettably,
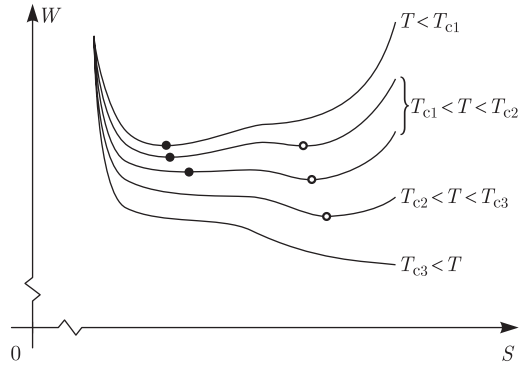
Figure 15   Free energy of a lipid molecule in the bilayer as a function of the molecular area, at five different temperatures. The units on both axes are arbitrary.
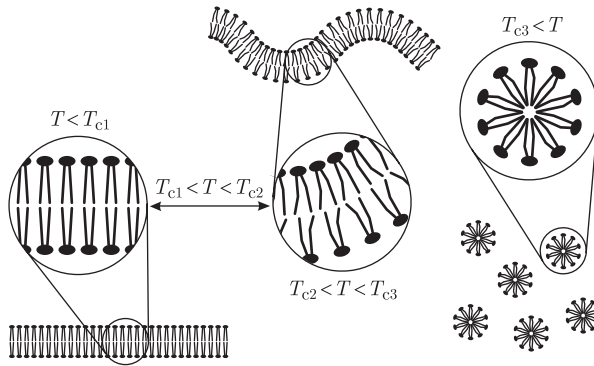
Figure 16   Membrane deformation and breakdown according to the phase transition model.

in the statistical mechanical model of Jacobs and co-workers, only $W_f(S)$ is an expression with a genuine physical basis, while the rest are polynomial regressions to the experimental data. In addition, the model contains several parameters with completely unknown actual values, and by adapting these one gets an arbitrarily good agreement with the experimental data. The specific formulae of the phase transition model are thus of little interest here, so we henceforth focus on the qualitative description it provides. Figure 15 illustrates this description by plotting the free energy per molecule as a function of the average area occupied per molecule, with the temperature serving as a parameter, and with arbitrary units on both axes.

As shown in Fig. 15, at temperatures below T_{c1}, the dependence of free energy on molecular area has a single minimum, which corresponds to the solid (gel) phase, which is the only possible stable state (Fig. 16, left). Between T_{c1} and T_{c2}, a second minimum occurs on the curve, corresponding to the liquid phase. In this temperature range, both phases can exist, but the one corresponding to the global minimum is more frequent. Above T_{c2}, the first minimum disappears, and the membrane can only persist in the liquid phase (Fig. 16, center). Finally, at

temperatures above T_{c3}, the remaining minimum also vanishes, and the membrane dissolves in the surrounding water, forming small micelles (Fig. 16, right). As an example, for a DPPC bilayer, $T_{c1} \approx 25\,°C$, $T_{c2} \approx 40\,°C$ and $T_{c3} \approx 165\,°C$ [1].

In the presence of a transmembrane voltage, the model described above has to be expanded by an additional component of the free energy, the electrical energy W_e, and the total free energy now becomes

$$W(T, S, U) = W_f(S) + W_c(T, S) + W_{ic}(T, S) + W_{ih}(T, S) + W_e(T, S, U) \quad (7)$$

where we assume that the electrical energy depends not only on the transmembrane voltage, but also on the temperature and the molecular surface area. In his model [72], Sugár derived the following approximation for $W_e(T, S, U)$:

$$W_e(T, S, U) = kT \log \frac{YS}{l\pi kT} - \frac{\varepsilon_m^2 S}{128 l^3 Y} U^4 \quad (8)$$

where k is the Boltzmann constant, T the absolute temperature, Y the elasticity module of the molecules in the direction of their hydrocarbon chains, S the average area of the molecules, l is the length of the hydrocarbon chains, ε_m is the dielectric permittivity of the molecules and U the transmembrane voltage. From this formula it is evident that at a sufficiently high transmembrane voltage, W_e becomes negative, shifting the entire free energy curve down, and this shift is more pronounced at higher molecular areas. Figure 17 shows this effect at a physiological temperature $T_{c1} < T < T_{c2}$ (for reasons described above, we again use arbitrary units for both axes). At a voltage U_{c1}, the first minimum of the free energy disappears, forcing the membrane into the liquid phase state. At a somewhat higher voltage U_{c2}, the remaining minimum also ceases to exist, leading to the breakdown of the membrane. The phases of the lipid membrane at various voltages are thus analogous to those at various temperatures presented in Fig. 16. Using numerical values for all the parameters of his model, Sugár calculated that for a DPPC bilayer, $U_{c1} \approx 260\,mV$ and $U_{c2} \approx 280\,mV$.

Comparison between Figs. 15 and 17 shows that according to the phase transition model, the presence of transmembrane voltage has an effect similar to
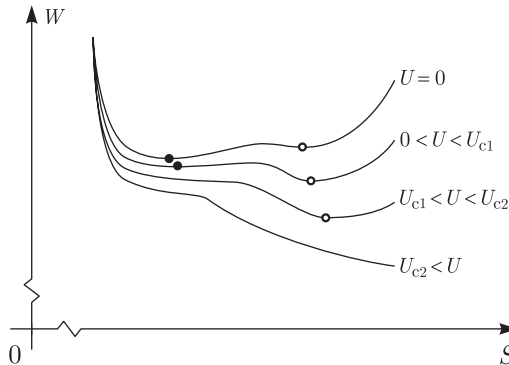
Figure 17 Free energy of a lipid molecule in the bilayer as a function of the molecular area, at four different transmembrane voltages. The units on both axes are arbitrary.

heating, causing a transition to the liquid phase, and eventually to decomposition similar to a high-temperature disintegration. Such a description is very unrealistic, since the permeabilized membrane is far from complete disintegration, and often returns to the nonpermeabilized state.

For an impartial evaluation of the predicted value of the critical transmembrane voltage, the parameters of the model which are at present arbitrary will have to be determined experimentally. In addition, this model is only provisional until the polynomial expressions obtained by regression are replaced by physical laws.

Still, the phase transition model meets several requirements at which all the previous models fail. The permeabilized state is the minimum of free energy, and the return to the nonpermeable state requires a sufficient input of energy, which offers a possible explanation of the observed durability of the permeabilized state. Similarly, the transition to this state requires a sufficient input of energy, which could explain the dependence on pulse duration. Above the second critical voltage, the downward slope of the free energy is never reversed, leading to a breakdown and explaining the limited reversibility of electropermeabilization. Except for the explanation of the dependence on the number of pulses, this model thus meets all the qualitative requirements from the list at the beginning of this chapter. This suggests that the approach based on the free energy could be a promising one.

3.6. The Domain-Interface Breakdown Model

The domain–interface breakdown model takes into account the fact that cell membranes can consist of distinct domains which differ in their lipid structure, particularly in their content of cholesterol. According to this model, elect–ropermeabilization is localized to the boundaries between the domains [88,89], as Fig. 18 schematically shows.

$U > U_t$ $U < U_t$
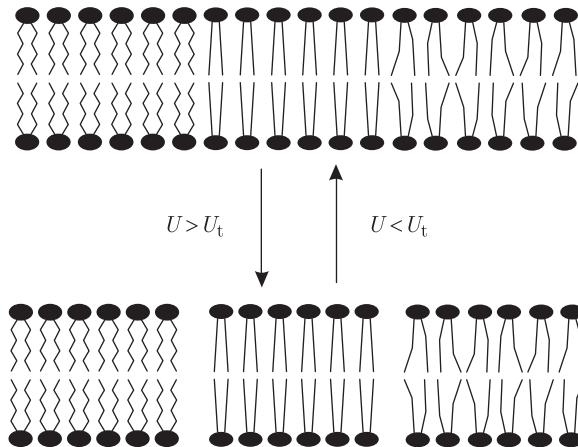
Figure 18   Membrane breakdown according to the domain–interface breakdown model.

Similarly to the viscohydroelastic model, in the domain-interface breakdown model the increased permeability is a result of fractures, with the difference that in the former model they occur along the ripples, while in the latter they form along the domain interfaces. As with the viscohydroelastic model, this description remains questionable, as such fractures have never been observed. In addition, while the model describes permeabilization as localized to the domain interfaces, the phenomenon is also observed experimentally in bilayers and vesicles with homogeneous lipid structure. Thus the domain-interface breakdown can only serve as an additional mechanism, perhaps enhancing permeabilization in cell membranes with respect to that in artificial bilayers and vesicles.

3.7. The Aqueous Pore Formation Model

The first four models treated here – the hydrodynamic, the elastic, the viscoelastic and the viscohydroelastic model – view electroporation as a large scale phenomenon, in which the molecular structure of the membrane plays no direct role.[1] The next two – the phase transition model and the domain-interface breakdown model – represent the other extreme, trying to explain the phenomenon by the properties of individual lipid molecules and interactions between them.

A compromise between these two approaches is offered by the model of pore formation, according to which electropermeabilization is caused by formation of transient aqueous pores (electroporation) in the lipid bilayer. In this model, each pore is formed (surrounded) by a large number of lipid molecules, but the shape, size and stability of the pore are strongly influenced by the structure of these molecules and their local interactions.

The model of pore formation is the last one to be described here, and in its present form, it is considered by many as the most convincing explanation of electropermeabilization. Therefore, in the following paragraphs an attempt will be made to follow its development rather comprehensively, from the first designs up to its current appearance.

The possibility of spontaneous pore formation in lipid bilayers was first analyzed in 1975, independently by two groups [90,91]. According to this analysis (which did not yet account for the effects of transmembrane voltage) formation of a cylindrical pore of radius r changes the free energy of the membrane by

$$\Delta W(r) = 2\gamma\pi r - \Gamma\pi r^2 \tag{9}$$

where γ is the edge tension and Γ the surface tension of the membrane. The first term, often termed the edge energy, is positive, since a pore creates an edge in the membrane, with a length corresponding to the circumference of the pore. The second term, the surface energy, is negative, as a pore reduces the surface area of the membrane. According to the above expression, the change of free energy is positive for small pores, and negative for sufficiently large pores. This implies that

---

[1] This point should not be obscured by the figures accompanying the models, in which separate lipid molecules are depicted. However, these figures combine the macroscopical description, which is actually provided by these models, with the existing knowledge of molecular structure of the lipid membrane.

spontaneous pore formation is inhibited by an energy barrier, explaining the stability of the membrane in the physiological conditions. The critical radius at which the energy barrier reaches a peak and the height of this peak are given by

$$r_c = \frac{\gamma}{\Gamma}, \quad \Delta W_c = \Delta W(r_c) = \frac{\pi\gamma^2}{\Gamma}. \tag{10}$$

Typical parameter values (Table 4) give $r_c \approx 10$ nm. If a larger pore is artificially created (e.g. by piercing the membrane), this energy barrier is overcome, and since no stable state exists at larger pore radii, the membrane breaks down.

In the presence of a transmembrane voltage, formation of a pore also affects the capacitive energy of the system. By accounting for this Abidor and co-workers obtained a more general expression for the change of the free energy [47],

$$\Delta W(r, U) = 2\gamma\pi r - \Gamma\pi r^2 - \frac{(\varepsilon_e - \varepsilon_m)\pi r^2}{2d} U^2. \tag{11}$$

where U is the transmembrane voltage, while ε_e and ε_m are the dielectric permittivities of the aqueous medium (in approximation, that of water) in the pore and the membrane. The transmembrane voltage reduces both the critical radius of the pore and the energy barrier, which are now given by

$$r_c(U) = \frac{\gamma}{\Gamma + \frac{\varepsilon_e - \varepsilon_m}{2d} U^2}, \quad \Delta W_c(U) = \Delta W(r_c, U) = \frac{\pi\gamma^2}{\Gamma + \frac{\varepsilon_e - \varepsilon_m}{2d} U^2}. \tag{12}$$

Applying parameters values from Table 4, Fig. 19 shows the free energy curves in absence and in presence of transmembrane voltage (solid) The voltage reduces the critical radius from $r_c \approx 10$ nm (outside the graph range) to $r_c \approx 1.93$ nm, i.e. to less than 20% of the value in the absence of transmembrane voltage, and the energy barrier is decreased in the same proportion.
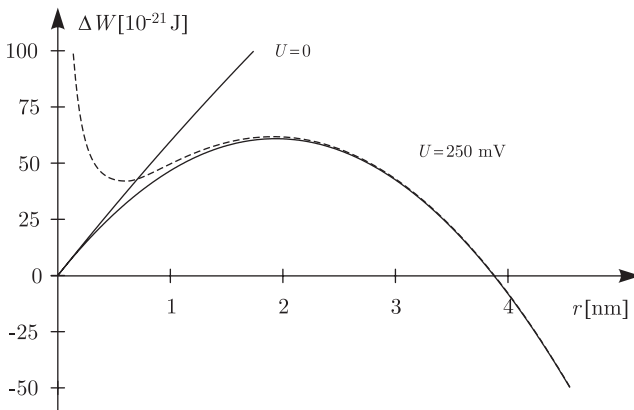
Figure 19   Free energy change due to the occurrence of a hydrophilic pore in the lipid bilayer, plotted as a function of the pore radius. The solid curves show the case of a constant edge tension, and the dashed curve the case where the edge tension increases as the pore radius decreases.
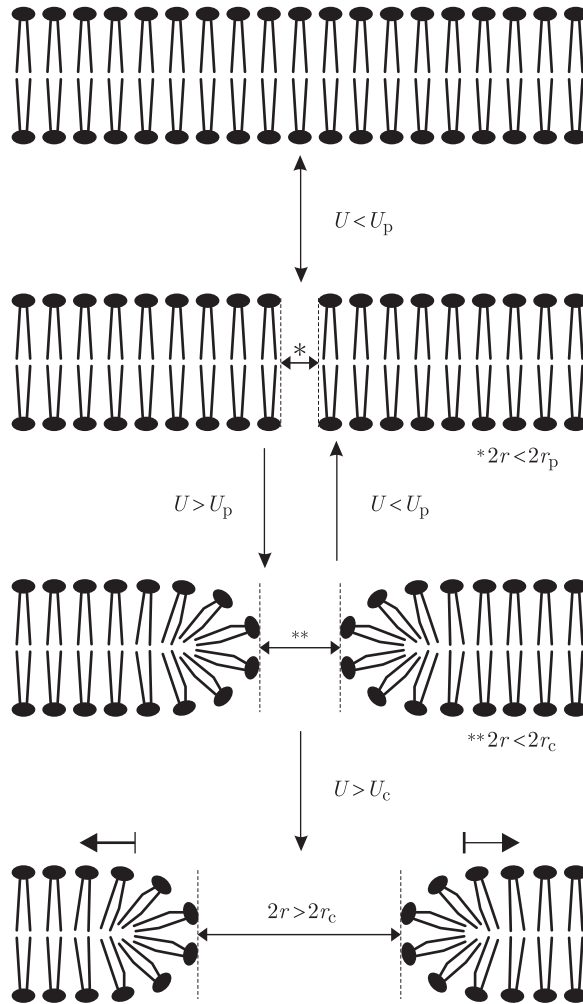
Figure 20 Formation of an aqueous pore according to the model of electroporation. From top to bottom: the intact bilayer; the formation of a hydrophobic pore; the transition to a hydrophilic pore and a limited expansion of the pore radius corresponding to a reversible breakdown; unlimited expansion of the pore radius corresponding to an irreversible breakdown.

Like many of the models presented before, this version of the model of pore formation fails to describe a permeabilized membrane, since according to it, an above-critical voltage causes a complete breakdown of the membrane. Another shortcoming of this model becomes evident from the structure of an aqueous pore (Fig. 20, bottom), where the lipids adjacent to the aqueous inside of the pore are reoriented in a manner that their hydrophilic heads are facing the pore, while their hydrophobic tails are hidden inside the membrane. Weaver and Mintzer argued that such a reorientation requires an input of energy which is larger for smaller pores [92], correspondingly increasing the free energy of the membrane at small pore radii

(Fig. 19, dashed). They suggested that this effect can be accounted for by treating the edge energy as a function $\gamma(r)$ the value of which becomes larger as the pore radius decreases,

$$\Delta W(r, U) = 2\gamma(r)\pi r - \Gamma\pi r^2 - \frac{(\varepsilon_e - \varepsilon_m)\pi r^2}{2d}U^2,\tag{13}$$

but they did not provide an expression for $\gamma(r)$.

The next step in the revision of the model of pore formation was a crucial one, as it described the stable state of a pore [46]. The argument that led to this revision is again illustrated in Fig. 20, where the hydrophilic structure of the pore is reached through a transition from an initial, hydrophobic state, in which the lipids still have their original orientation. The expressions for ΔW given so far do not deal with this transition, and at all radii they treat the pore as fully formed, i.e. hydrophilic. Glaser and co-workers argued that up to the pore radius r_p at which the hydrophilic state forms, the free energy change due to a hydrophobic pore must be analyzed instead, for which they derived the expression (see Appendix A.5)

$$\Delta W(r, U) = 2\pi dr \Gamma_h \frac{I_1(r/\lambda)}{I_0(r/\lambda)},\tag{14}$$

where Γ_h is the surface tension at the interface of the hydrophobic internal surface of the pore and water, λ is the characteristic length of hydrophobic interactions, and I_k denotes the modified Bessel function of k-th order. As in the hydrophilic case, the total change of free energy also reflects the decrease of the membrane surface and the electric energy. The change of free energy of the membrane accompanying electroporation can thus be described by the system of two equations

$$\Delta W(r, U) = \begin{cases} 2\pi dr \Gamma_h \dfrac{I_1(r/\lambda)}{I_0(r/\lambda)} - \Gamma\pi r^2 - \dfrac{(\varepsilon_e - \varepsilon_m)\pi r^2}{2d}U^2; & r < r_p \\[4mm] 2\pi r\gamma(r) - \Gamma\pi r^2 - \dfrac{(\varepsilon_e - \varepsilon_m)\pi r^2}{2d}U^2; & r > r_p \end{cases}\tag{15}$$

The pore radius r_p at which the transition from the hydrophobic to the hydrophilic state occurs corresponds to the intersection of the hydrophilic and the hydrophobic branch of ΔW, but as $\gamma(r)$ is not defined, it is also impossible to give an explicit formulation of r_p.

Using $\lambda = 1$ nm [93], $\Gamma_h = 0.05$ N/m [46] and other values as in Table 4, we can plot both branches of ΔW on the same graph, as shown in Fig. 21. For transmembrane voltages of 250 and 350 mV, the solid lines give the curve into which the hydrophobic and the hydrophilic branch combine, and the dashed lines are the extrapolations of these two branches beyond their actual domains. Regrettably, a local minimum of free energy only occurs if the hydrophilic branch contains a suitable form of the (unknown) function $\gamma(r)$.

The model of pore formation as illustrated by Figs. 20 and 21 represents what is today referred to as the aqueous pore formation model (or simply as "the standard model of electroporation"), where the phenomenon is defined as formation of aqueous pores in the presence of transmembrane voltage. In this model,
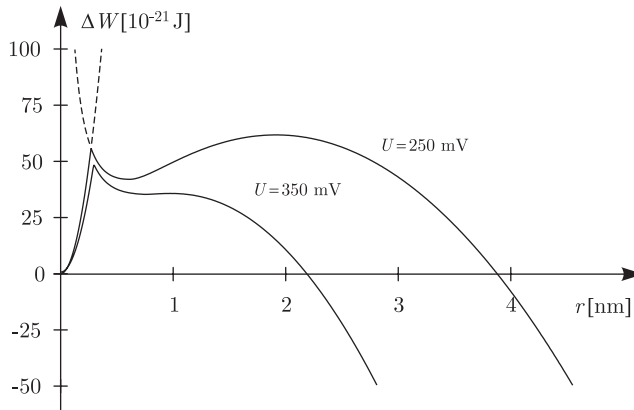
Figure 21 Free energy change due to the formation of an aqueous pore, plotted as a function of the pore radius. The initial increase corresponds to the formation and expansion of a hydrophilic pore, the local maximum to the transition to a hydrophilic pore, and the subsequent local minimum corresponds to the radius of a (semi-) stable hydrophilic pore. At sufficiently high transmembrane voltages, this minimum transforms into a monotonic decrease, which corresponds to an irreversible breakdown.

transmembrane voltage decreases the energy input necessary to induce a transition from the hydrophobic[2] to the hydrophilic state. The hydrophilic pores correspond to a local minimum of free energy, and are thus stable, which could possibly explain the experimentally observed durability of the permeabilized state. Reversibility of this state is limited as at voltages above the critical value there is an irreversible breakdown of the membrane. Qualitatively, also the dependence of elect-ropermeabilization on pulse duration is explained, since pore formation requires a sufficient input of energy for the transition to the hydrophilic state. In the models of pore formation, including the aqueous pore formation model of electroporation, the transmembrane voltage does not cause, but only facilitates the formation of hydrophilic pores, which can account for the stochasticity of electropermeabilizat-ion. As Figs. 19 and 20 testify, the values at which this facilitating effect becomes pronounced are in hundreds of millivolts, and thus in relatively good agreement with the experiments.

Still, the aqueous pore formation model of electroporation has two significant shortcomings. The first is clearly observable in Fig. 21; namely, with realistic pa-rameter values applied, the transmembrane voltage reduces the energy barrier of the hydrophobic–hydrophilic transition, but it reduces the barrier of an irreversible breakdown to a much larger extent. For example, a transmembrane voltage above 361 mV reduces the energy barrier of aqueous pore formation by only several percent, but once the pore is formed, this voltage imminently leads to the break-down. This effect is independent of the choice of the arbitrary function $\gamma(r)$, since it is governed exclusively by the contribution of the electric energy. Nonetheless, the

---

[2] Because of the lateral thermic fluctuations of the lipid molecules, hydrophobic pores, with lifetimes in the picosecond range, are in certain extent always present in the membrane.

undefined functional form of $\gamma(r)$ is the second shortcoming of the aqueous pore formation model of electroporation. In absence of its definition, the expressions for the energy barrier that impedes the hydrophobic–hydrophilic transition, as well as the minimum radius of a hydrophilic pore r_{p} also remain undefined. This short-coming will probably be addressed in the future, either theoretically, by a derivation of a physical law which would define $\gamma(r)$, or experimentally, by a measurement of its values. On the long term, the former alternative is definitely preferred.

Subsequent paragraphs contain a short overview of various extensions of the aqueous pore formation model that have been proposed by different authors.

3.8. Extensions of the Aqueous Pore Formation Model

Several approaches have been proposed for improving the aqueous pore formation model presented in the preceding section. Two of these [94,95] addressed its du-bious prediction that transmembrane voltage strongly facilitates an irreversible breakdown. Barnett and Weaver accounted for the fact that a pore alters not only the capacitive, but also the conductive energy of the membrane, and reformulated the electric energy as[3]

$$\Delta W_{\mathrm{e}} = -\frac{(\varepsilon_{\mathrm{e}} - \varepsilon_{\mathrm{m}})\pi}{d} U^2 \int_0^r \frac{\rho \, d\rho}{(1 + \lambda(\rho))^2} \tag{16}$$

with

$$\lambda(\rho) = \frac{\pi\rho\sigma_{\mathrm{p}}}{2d\sigma_{\mathrm{e}}} \tag{17}$$

where σ_{e} and σ_{p} are the electric conductivities of the aqueous medium outside and inside the pore. The exact value of σ_{p} depends on the properties of the lipid headgroups forming the surface of the pore, as well as on the properties of the aqueous medium inside the pore, but in the first approximation it is reasonable to assume that $\sigma_{\mathrm{p}} \approx \sigma_{\mathrm{e}}$, so that

$$\lambda(\rho) = \frac{\pi\rho}{2d} \tag{18}$$

and the electric energy is given by

$$\Delta W_{\mathrm{e}} = -(\varepsilon_{\mathrm{e}} - \varepsilon_{\mathrm{m}}) \, U^2 \left(\frac{4d \log\left(1 + \frac{\pi r}{2d}\right)}{\pi} - \frac{2r}{1 + \frac{\pi r}{2d}} \right). \tag{19}$$

Figure 22 compares, for a transmembrane voltage of $350\,\mathrm{mV}$, the free energy change as a function of pore radius with (solid) and without (dashed) the described modification of the electric energy. The revised curve of free energy change shows a significantly broadened range of stable pore radii. The voltage which leads to an irreversible breakdown is shifted up to $\approx 458\,\mathrm{mV}$, which is an improvement with respect to the previous value of $\approx 361\,\mathrm{mV}$, but is still rather low. Also in the revised

---

[3] Note that using $\lambda(\rho) = 0$, we get ΔW_{e} of the standard model (i.e. the result derived by Abidor and co-workers).
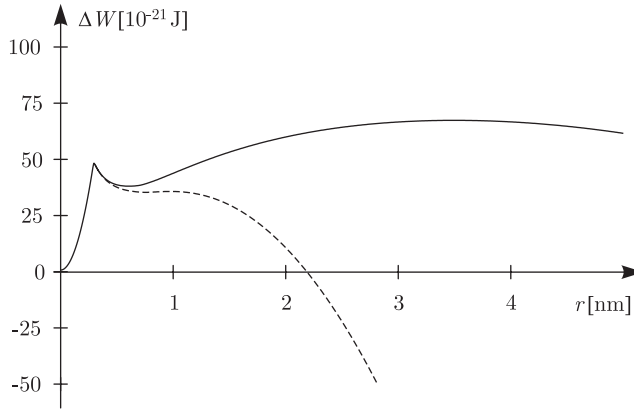
Figure 22 Free energy change as a function of the pore radius, without (dashed) and with (solid) the modification of the conductive electric energy as formulated by Barnett and Weaver [94].

model, the facilitating effect of transmembrane voltage on formation of aqueous pores remains very weak.

Freeman and co-workers [95] made an attempt to enhance this model further by accounting for the energy needed by charged particles to traverse the pore (the Born energy), which led them to a more complicated expression for $\lambda(\rho)$ expressed as a polynomial regression of experimental data.

Another study has addressed the effect of the difference between the osmolarities of the extracellular medium and the cytoplasm [32]. To address this effect, the change of free energy must incorporate the change of osmotic energy caused by the pore formation,

$$\Delta W_{\mathrm{osm}} = -\frac{|p_{\mathrm{e}} - p_{\mathrm{i}}|R}{2}\pi r^2 \tag{20}$$

where p_{e} and p_{i} are the osmotic pressures in the extracellular medium and inside the vesicle or cell, respectively, and R is the radius of the vesicle or cell. The osmotic energy thus acts similarly to the surface energy and the electric energy – it reduces the free energy of the membrane, and is proportional to r^2. This implies that a difference between the osmolarities makes the membrane more susceptible to the effects of the transmembrane voltage, which seems to be in agreement with experiments [96,97].

Finally, it was also analyzed how electroporation is affected by the curvature of the membrane [98]. Unlike in planar bilayers, in vesicles and cells the membrane is inherently curved, with the curvature increasing with a decreasing cell radius. According to the calculations by Neumann and co-workers, the change of curvature energy caused by the pore formation is

$$\Delta W_{\mathrm{crv}} = -\frac{64Y}{Rd}\pi^2 r^2 \tag{21}$$

where Y is the elasticity module of the membrane and R the radius of the cell. This also shows that the curvature reduces the free energy of the membrane and implies that, at a given transmembrane voltage, electroporation is more intense in smaller cells.[4]

Today, many consider the aqueous pore formation model to be the most convincing explanation of electroporation. If in the future it preserves this status, then further research, especially measurements of the relevant physical quantities, should gradually result in the improvement of the current form of the aqueous pore formation model. It is reasonable to expect that some of the tentative extensions described above will soon be incorporated into the model, while revisions and entirely new propositions will continue to appear. It is also reasonable to expect that an explicit formulation of the function $\gamma(r)$ should be given in the near future. The insights obtained by molecular dynamics simulations, and perhaps by an advanced method of visualization or another type of detection, should also yield a clearer picture of the electropermeabilized membrane on a nanometer scale, thereby providing the final verdict on the validity of the concept of electroporation.

4. Electroporation of Cells-Experimental Observations and Analysis of Underlying Phenomena

The electroporation of cells is sometimes also referred to as electropermeabilization, which stresses the crucial observation that increased permeability of the cell membrane is observed above a certain critical (threshold) applied electric field. It was shown by several independent studies that electroporation of cells is closely related to electroporation of lipid bilayer membranes, referred to also as dielectric breakdown, and that the structural changes in the membrane are formed in the lipid part of the cell membrane. Still the exact molecular mechanisms of the formation, structure and stability of these permeable structures (pores) are not completely understood [32,99]. On one hand the theoretical descriptions that were developed for lipid bilayers do not include cell structures such as cytoskeleton and proteins. In addition non of the existing theories can describe permeable structures or pores which could be stable for minutes and hours after pulse application. On the other hand, the increased permeability after the pulses, which enables delivery of molecules (drugs, DNA molecules …) is crucial for application of cell electroporation in biotechnology in biomedicine [2,100,101]. Therefore, phenomenological observations and quantification of cell electroporation can lead to some conclusions enabling evaluation of electroporation theories when applying them to such complex systems as cells and helps to understand the underlying mechanisms.

For this reason, we will present the theoretical and experimental data on the electroporation of cells. We will focus on the experimental evidence of cell

---

[4] This is true for a given transmembrane voltage, but not for a given pulse amplitude, since the transmembrane voltage induced by the pulse is proportional to the cell radius.

electroporation *in vitro* and on related theoretical interpretations. First, we briefly present theoretical descriptions of phenomena involved in cell electroporation: the induced transmembrane potential, forces which act on the cell and the transport which occurs through permeabilized cell membrane. Then we will overview several experimental studies, which studied different involved phenomena (imaging, conductivity, transport of molecules …), and finally we discuss how the theoretical description of pore formation presented in previous section can be applied to experimental observations of cell electroporation.

4.1. Induced Transmembrane Voltage and Forces on the Cell Membrane

Even though the exact physical–chemical mechanisms of cell electroporation are not clear and several theoretical models exist, it is generally accepted that one of the key parameters for successful permeabilization is the induced transmembrane voltage. This voltage is generated by an external electric field due to the difference in the electric properties of the membrane and the external medium, known as the Maxwell–Wagner polarization [102,103]. If the induced transmembrane voltage is large enough, i.e. above the critical value, electroporation is observed – a cell membrane becomes permeabilized in a reversible process allowing easier transport of ions and entrance of molecules that otherwise cannot easily cross the cell membrane [2,6,7,29,32,101].

4.1.1. The induced transmembrane voltage on a spherical cell
We consider a spherical cell exposed to an external homogeneous electric field E_0, as schematically shown in Fig. 23, where R denotes radius of the cell, d thickness of the membrane, conductivities σ and ε permittivities of the cell membrane, cytoplasm and exterior (Table 5).

The Laplace equation holds for all three regions: e – external medium, m – membrane and i – the cell interior. The respective potentials satisfying Laplace's
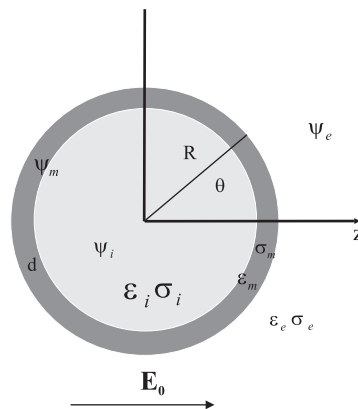
Figure 23 A spherical cell in external electric field.

Table 5 Typical values of conductivity and permittivities of a cell [104].

	Conductivity	Permittivity
External medium	$^a\sigma_e = 1.2\,\text{S/m}$	$\varepsilon_e = 7.1 \times 10^{-10}\,\text{As/Vm}$
Cytoplasm	$\sigma_i = 0.5\,\text{S/m}$	$\varepsilon_i = 7.1 \times 10^{-10}\,\text{As/Vm}$
Membrane	$\sigma_m = 10^{-7}\,\text{S/m}$	$\varepsilon_m = 4.4 \times 10^{-11}\,\text{As/Vm}$
Membrane thickness	$d = 5 \times 10^{-9}\,\text{m}$	
Cell radius	$R = 10^{-5}\,\text{m}$	

^{a}Physiologycal saline

equation are given by following expressions [105]:

$$\Psi_e = E_0 r \cos\theta - \frac{a}{r^2} E_0 \cos\theta \tag{22}$$

$$\Psi_m = A E_0 r \cos\theta - \frac{B}{r^2} E_0 \cos\theta \tag{23}$$

$$\Psi_i = C E_0 r \cos\theta \tag{24}$$

where r and θ are spherical coordinates. The boundary conditions at two borders–inner radius (R_1) and outer radius (R), representing the conservation of the current:

$$\sigma_e \left.\frac{\partial \psi_e}{\partial r}\right|_R = \sigma_m \left.\frac{\partial \psi_m}{\partial r}\right|_R, \quad \sigma_m \left.\frac{\partial \psi_m}{\partial r}\right|_{R_1} = \sigma_i \left.\frac{\partial \psi_i}{\partial r}\right|_{R_1} \tag{25}$$

and potential:

$$\psi_e|_R = \psi_m|_R, \quad \psi_m|_{R_1} = \psi_i|_{R_1} \tag{26}$$

define a set of four linear equations for the constants a, A, B and C. By solving the above set of equations [2] and taking into account that for cells $d \ll R$ we obtain the expression for the induced transmembrane voltage:

$$U_m = \Delta\Psi = \frac{3}{2} E_0 R \cos\theta \frac{3\frac{d}{R}\sigma_i\sigma_e}{(\sigma_m + 2\sigma_e)(\sigma_m + \frac{1}{2}\sigma_i) - (1 - \frac{3d}{R})(\sigma_e - \sigma_m)(\sigma_i - \sigma_m)} \tag{27}$$

which can be further simplified if the membrane conductivity is much smaller than external and internal conductivity (true for physiological conditions):

$$U_m = \Delta\Psi = \frac{3}{2} E_0 R \cos\theta. \tag{28}$$

The induced transmembrane voltage has maximum at both cell poles and is proportional to the external electric field and cell diameter. From the transmembrane voltage we can obtain the electric field inside the membrane $E_m = U_m/d$, which is amplified for a factor of $R/d(\sim 10^3)$. And predominately this strong electric field inside the cell membrane is crucial for structural changes inside the lipid bilayer.

Most of the authors agree [29,106–108] that the induced transmembrane voltage is superimposed on the resting transmembrane voltage, resulting in an asymmetric transmembrane voltage. The above equation gives the induced transmembrane voltage for a spherical cell, which is valid for cells for most of the conditions present in experiments and is widely used in the literature. However, there are some cases where this simplified equation leads to considerable errors: for very low-conductive media $\sigma_e < 0.01$ S/m [109,110] the original equation has to be used where all three conductivities influence the induced transmembrane voltage. The above derivation follows from Laplace equation, which is valid only if the electroneutrality condition is satisfied (no net charges in any of the regions). This is not true for a biological cell where surface charge is present in a layer with thickness of a Debye length. Thus, instead of the Laplace equation the Poisson equation should be solved. The difference between the solutions of both equations is significant only for very low-conductive media and can be neglected otherwise [2,111].

Schwan derived the time dependent solution [109] for the induced transmembrane voltage on a spherical cell for a step turn-on of a DC electrical field:

$$\Delta\Psi = \frac{3}{2} E_0 R \cos\theta \left(1 - e^{-t/\tau}\right) \frac{3\frac{d}{R}\sigma_i\sigma_e}{(\sigma_m + 2\sigma_e)(\sigma_m + \frac{1}{2}\sigma_i) - \left(1 - \frac{3d}{R}\right)(\sigma_e - \sigma_m)(\sigma_i - \sigma_m).} \quad (29)$$

The time constant τ also depends on the dielectric properties of the membrane:

$$\tau = \frac{\varepsilon_m}{\dfrac{d}{R}\dfrac{2\sigma_e\sigma_i}{2\sigma_e + \sigma_i} + \sigma_m} \quad (30)$$

where ε_m denotes permittivity of the membrane. The time constant τ represents a typical time needed for charging of a cell membrane, which behaves as a capacitor. It is directly related to the frequency of beta dispersion observed in impedance spectra of cells. For a typical biological cell we obtain a time constant around a microsecond, which represents the time that is needed for the induced transmembrane voltage to build up on the cell membrane and for electroporation to occur. For times shorter than microsecond the cell interior is also exposed to an electric field, resulting in the induced transmembrane voltage across the membrane of the cellular organelles. Thus for very short high-voltage pulses cell organelles can be permeabilized [112]. The above equation is valid for the response of a cell to a square pulse, however, for other pulse shapes the responses differs from the exponential [113].

4.1.2. Dense cell systems

In case of dense cell systems (dense suspension and tissue) with high cell volume fraction ($f > 0.1$) [114,115] the local electric field E is lower than the applied electric field E_0 due to the effect of neighboring cells. In Fig. 24 it can be seen that in case when $f = 0.5$ normalized induced transmembrane voltage is decreased from 1.5 to 1.3 for cells organized in fcc lattice, which is the most realistic representation of cell ordering in dense suspension. Therefore in dense cell suspensions and tissue the decrease in the local field should be taken into account.
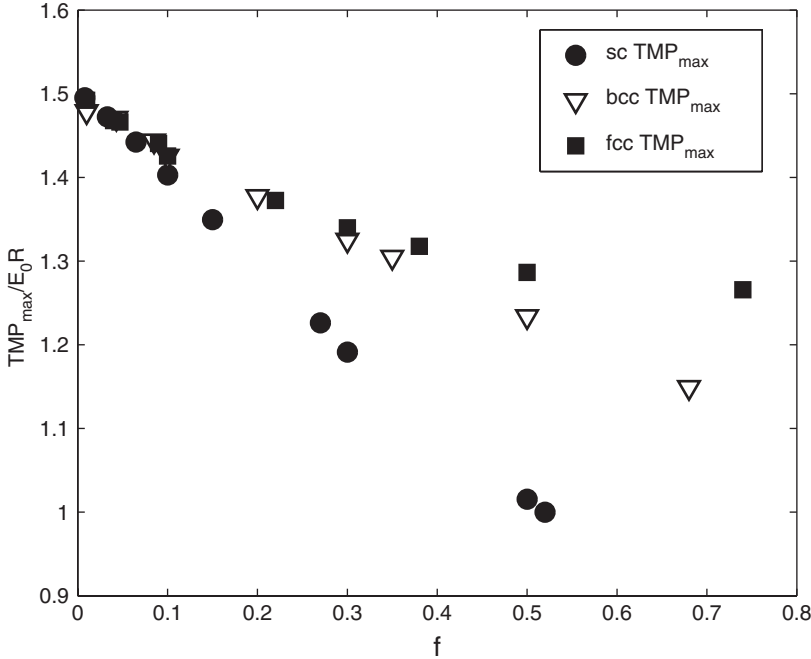
Figure 24   The normalized maximal ($\phi = 0°$) induced transmembrane voltage-$\text{TMP}_{\text{max}}/E_0 R$ in dense cell suspension (f-cell volume fraction) for three different cubic lattices (simple cubic – sc, body centered cubic – bcc and face centered cubic lattice – fcc).

4.2. Maxwell Stress Tensor and Forces Acting on a Cell in an External Field

The cell membrane experiences different forces in the presence of an external electrical field, which can be derived from Maxwell stress tensor:

$$T_{ij} = \varepsilon \left(E_i E_j - \tfrac{1}{2} E^2 \delta_{ij} \right). \tag{31}$$

From the solution of a Laplace equation for a cell in an external field E_0 (equations (22–24)) we can calculate the electric fields in the cytoplasm, membrane and outside the cell [2]. For the average radial component of the field inside the membrane we obtain:

$$E_{\text{rm}} = \frac{3}{2} \frac{R(1 - 2d/R)}{d} E_0 \cos\theta \approx \frac{3}{2} \frac{R}{d} E_0 \cos\theta \tag{32}$$

and for radial components inside and outside the cell:

$$E_{\text{ri}}(R_1) = 3 E_0 \frac{\sigma_m \sigma_e}{(2\sigma_m \sigma_e + \sigma_m \sigma_i) + 2\sigma_i \sigma_e d/R} \cos\theta \approx 3 E_0 \frac{\sigma_m R}{\sigma_i d} \cos\theta \tag{33}$$

$$E_{\text{re}}(R) = 3 E_0 \frac{\sigma_m \sigma_i \left(1 - 2d/R\right)}{(2\sigma_m \sigma_e + \sigma_m \sigma_i) + 2\sigma_i \sigma_e d/R} \cos\theta \approx 3 E_0 \frac{\sigma_m R}{\sigma_e d} \cos\theta. \tag{34}$$

If we insert the above equations into the expression for Maxwell stress tensor:

$$T_{ij} = \varepsilon\left(E_i E_j - \tfrac{1}{2}E^2\delta_{ij}\right) \tag{35}$$

we obtain the compression force in the membrane:

$$T_{rr}^m = \varepsilon_m E_{rm}^2/2 = \frac{9}{8}\left(\frac{R}{d}\right)^2 \varepsilon_m E_0^2\cos^2\theta. \tag{36}$$

Additionally, each surface experiences slightly different pressure yielding a net outward-directed force which tends to elongate the cell in the direction of the field:

$$T_{rr}^e - T_{rr}^i = \frac{9}{2}\frac{R}{d}\varepsilon_m E_0^2\cos^2\theta. \tag{37}$$

The elongation due to Maxwell stress tensor can be observed for giant vesicles under the microscope [116] for electric fields used in electroporation, however for cells the cytoskeleton prevents cells to deform. Only in case of extremely strong electric fields (above $10\,kV/cm$) that are used for electroporation of organelles with nanosecond pulses, some deformation of cells can be observed [117,118].

4.3. Transport of Molecules Across Permeabilized Membrane

In this section, we discuss the underlying mechanisms which contribute to the increased transport for ions, molecules and macromolecules across an electropermeabilized membrane. There are several possible transmembrane transport mechanisms of which most important are diffusion, electrophoresis, electroosmosis and osmosis. Which mechanism is dominant depends on the type of the object (ion, molecule), the length of the pulses, electric field strength, concentration gradients and other physical parameters. However, general observation in different experimental studies was that transport of ions and molecules occurs only through the permeabilized area.

4.3.1. Diffusion

The flux of a given neutral molecule through the permeable membrane can be described by diffusion equation:

$$\frac{dn_e(t)}{dt} = -\frac{c_e(t) - c_i(t)}{d}\,D f_{per}(t, E, t_E, N)\,S_0 \tag{38}$$

where f_{per} represents the fraction of pores in the cell membrane which is a complex function of time (t) (mostly due to resealing process), electric field strength (E), pulse duration (t_E) and number of pulses (N). Additionally, the diffusion constant for a given molecule depends on the size of permeable structures (pores), leading to an equation which in real experimental observations of molecular uptake can be used only approximately. The above equation can also describe diffusion of ions or charged molecules through the permeabilized region since diffusion is a relatively slow process which occurs mainly after the pulse application and thus the Nernst–Planck equation (see equation (90)) simplifies to the above equation.

4.3.2. Electrophoresis

Electrophoresis is another mechanism of transport which was shown to be the most important for the transport of charged macromolecules, especially for DNA molecules. The electrophoretic driving force acts on the charged molecules in the electric field, thus, unlike diffusion, is present only during the pulse. For this reason protocols for gene transfection use much longer pulses (a few to tens of milliseconds) than pulses used for uptake of smaller molecules, or combination of short high-voltage and long low-voltage pulses [119–121]. Electrophoretic force is the driving force for all charged molecules:

$$F = e_{eff} E_{loc} \tag{39}$$

where e_{eff} is the effective charge of a given molecule and E_{loc} the local electric field. The effective charge depends on the charge of a given molecule and on the ionic strength of the solution. The velocity of a given molecule depends on its mobility and viscosity of the medium.

4.3.3. Osmosis and electroosmosis

The osmotic flow is driven by the difference in the osmotic pressure inside and outside of the cell:

$$\Phi(t) \propto c(t)\, \Delta p \tag{40}$$

depending also on the permeability of the membrane. In most experimental conditions isoosmolar media are used, however, when a cell membrane is permeabilized, ions and smaller molecules are free to move due to diffusion, whereas macromolecules are bound inside the cell. Consequently, the cell interior is not in osmotic equilibrium with the exterior and thus water flowing into the cell causes its swelling. This swelling, also named colloid-osmotic swelling, is observed in electroporation experiments on cells [122–125]. Together with the flow of water also the molecules are driven into the cell.

Electroosmosis is the transport of bulk liquid through a pore under the influence of an electric field. In an electric field ions migrate together with their sheath of water molecules, which induces the flow of water through the pore.

4.3.4. The permeabilized surface area

Independently on the process it was shown that the transport of ions and molecules during electroporation occurs only through the permeabilized area S_c, i.e. the area which is exposed to above-critical voltage [84,126–128]. From the expression for the induced transmembrane voltage for an isolated spherical cell (equation (28)) we can define the critical angle θ_c where the induced voltage equals the critical voltage U_c:

$$\Delta U_c = \Delta\Psi = 1.5\, ER\cos\theta_c. \tag{41}$$

If we neglect the resting transmembrane voltage we obtain the formula for the area of two spherical caps (see Fig. 25) where $\Delta\Psi > U_c$:

$$S_c = 2 \times 2\pi R^2 (1 - \cos\theta_c). \tag{42}$$
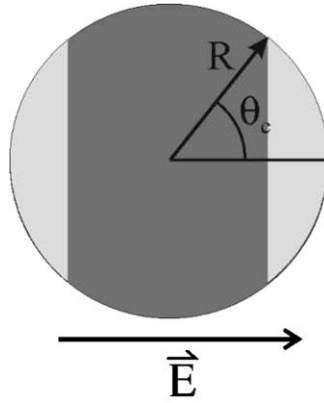
Figure 25 Schematical representation of permeabilized area of cell membrane.

Now, we define the critical field as the electric field when $\theta_c = 0$: $E_c = U_c/1.5$ and thus obtain the total area exposed to above-threshold transmembrane voltage:

$$S_c = S_0(1 - E_c/E). \tag{43}$$

When considering the flow of molecules and ions across the permeabilized membrane above equation has to be incorporated in order to determine total flow across the membrane. Therefore, part of electric field dependence of pore fraction f_{per} is due to the increased permeabilized surface.

4.4. Experimental Studies and Theoretical Analysis of Cell Electroporation *in vitro*

Different studies analyzed cell electroporation *in vitro* either on single cells as well as on attached cells, cells in suspensions or multicell spheroids. Common observation is that electroporation is a threshold phenomenon and that it is governed by pulse parameters (duration, number and repetition frequency). Sometimes the critical voltage (or applied field) above which the transport is observed is defined as the reversible threshold since the changes are reversible and the cell membrane reseals after a given time lasting from minutes to hours. The value of the critical (threshold) transmembrane voltage at the room temperature was reported to be between 0.2 and 1 V [29,31,85,108] depending on pulse parameters and experimental conditions [129]. Further increase of the electric field causes irreversible membrane permeabilization and cell death due to direct physical loss of membrane integrity or due to excessive loss of the cell interior content.

4.4.1. Imaging of the transmembrane voltage during electroporation
Kinosita, Hibino and co-workers [84] used fast video imaging on a microsecond time scale to measure transmembrane voltage of sea urchin eggs during and after the
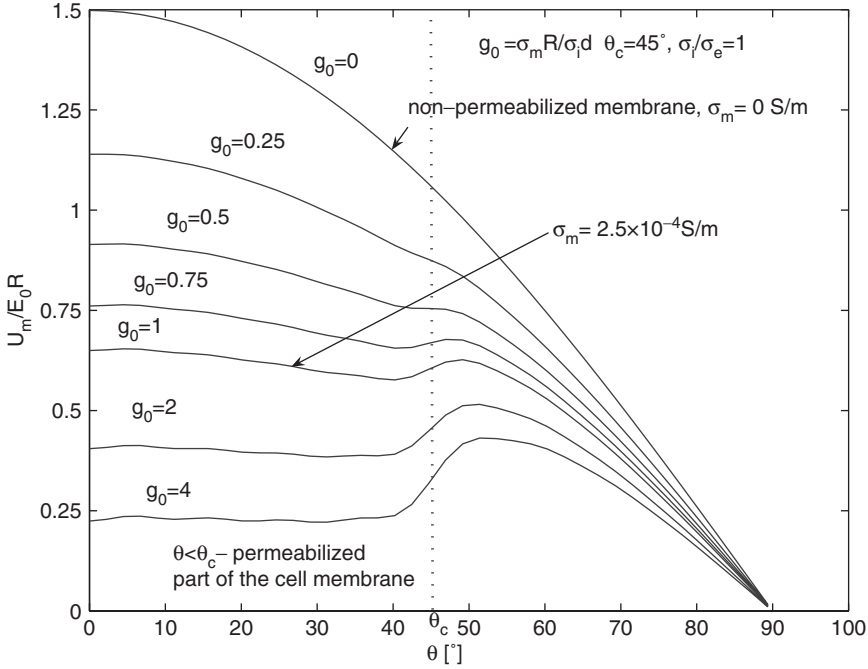
Figure 26   Analytically calculated normalized induced transmembrane voltage (TMP/E_0R) on a permeabilized cell for different maximum membrane conductivities g_0, $v = \sigma_i/\sigma_e$ [130]. Note that $g_0 = 1$ corresponds to $\sigma_m = 2.5 \times 10^{-4}$ S/m, a value of a permeabilized cell and $g_0 = 0$ to nonpermabilized membrane.

electric pulses. They observed a decrease of a cosine profile due to the increased specific membrane conductance, which they estimated to be around few S/cm^2. In the same study the authors also studied the kinetics of resealing and obtained two time constants: one of a few microseconds and the second time constant around a millisecond. This was compared to analytical model of an electroporated cell which also predicts a decrease in induced transmembrane voltage on a electroporated cell of which the membrane at the two pole caps has increased conductivity (see Fig. 26). The parameter g_0 is the normalized maximal membrane conductance at the two poles of the cell, defined as:

$$g_0 = \frac{\sigma_m}{\sigma_i} \frac{R}{d}. \tag{44}$$

Their experiments and analysis clearly showed that there exist conductive pathways during cell electroporation, which increase conductivity and decrease the induced transmembrane voltage in the area that is permeabilized. In the following study [85] they further showed that there exist at least two mechanisms for membrane resealing, where the slower process in the order of minutes enables a successful uptake of molecules following the application of pulses.

4.4.2. Measurements of conductivity in cell suspensions and pellets – quantification of short-lived pores

The first measurements of electrical properties of cells in a suspension during electroporation were done by Kinosita and Tsong [122,131,132], who measured electric properties of the isotonic suspension of erythrocytes. They observed an increase in the conductivity for electric fields around kV/cm and explained it with the increased membrane permeability for the ions due to formation of pores in a cell membrane. The initial step of pore formation was governed by the magnitude of the transmembrane voltage. From the measured changes of conductivity using their theoretical model they calculated the membrane conductivity and estimated the number of pores and ion flux through the permeabilized membrane. They determined that conductivity increased in two steps: a fast step in the range of one microsecond and a slower step which takes around 100 s. Specific membrane conductance increased up to $100\,S/cm^2$ but, in general, depended on pulse duration and electric field strength. After the end of the pulse the conductivity of the cell suspension returned to its initial value in a few seconds, but later on again increased due to the ion efflux. These observations were confirmed by the experiments of Abidor and co-authors [123,124] on cell pellets of different cell types, where an increase in the pellet conductance during the pulses above the critical electric field for electroporation was observed. After the pulse the conductance returned to the initial level in several stages: the first stage lasted milliseconds, the second a few seconds and the complete resealing was observed after minutes. They also observed changes of conductance due to the osmotic swelling of cells. Using microsecond and nanosecond pulses, several following studies observed increased conductivity during electroporation *in vitro* and *in vivo* [133,134] which suggested that measurement of conductivity could enable on-line observation and control of tissue electroporation [125,135,136].

Recently we made an extensive *in vitro* study of conductivity during cell electroporation of cell (B16F1 cells) suspensions. Figure 27 represents transient conductivity changes $\Delta\sigma_{\mathrm{tran}}{}^{N}/\sigma_0$ during the N-th pulse for $E_0 = [0.4$–$1.8]\,kV/cm$. An increase in transient conductivity changes is observed above $0.5\,kV/cm$, which is in agreement with the threshold for permeabilization of B16 cells obtained for molecular uptake. Interestingly, the number of pulses does not influence the transient conductivity [125,137].

From the measured conductivity changes fraction of the surface area of pores can be determined. Detailed derivation is presented in Appendix B.1. The fraction of transient pores f_{p} can be estimated as:

$$f_{\mathrm{p}} = \frac{S_{\mathrm{por}}}{S_0} \approx \frac{(1 - E_{\mathrm{c}}/E)\,\sigma_{\mathrm{m}}}{\rho\,\sigma_{0\mathrm{por}}} \tag{45}$$

where $\sigma_{0\mathrm{por}}$ is the average conductivity between inside the cell and extracellular medium and parameter ρ is:

$$\rho = \frac{1}{\left(1 + \frac{n\beta U_{\mathrm{m}}}{w_0 - n\beta U_{\mathrm{m}}}\right)\exp(w_0 - n\beta U_{\mathrm{m}}) - \frac{n\beta U_{\mathrm{m}}}{w_0 - n\beta U_{\mathrm{m}}}}. \tag{46}$$
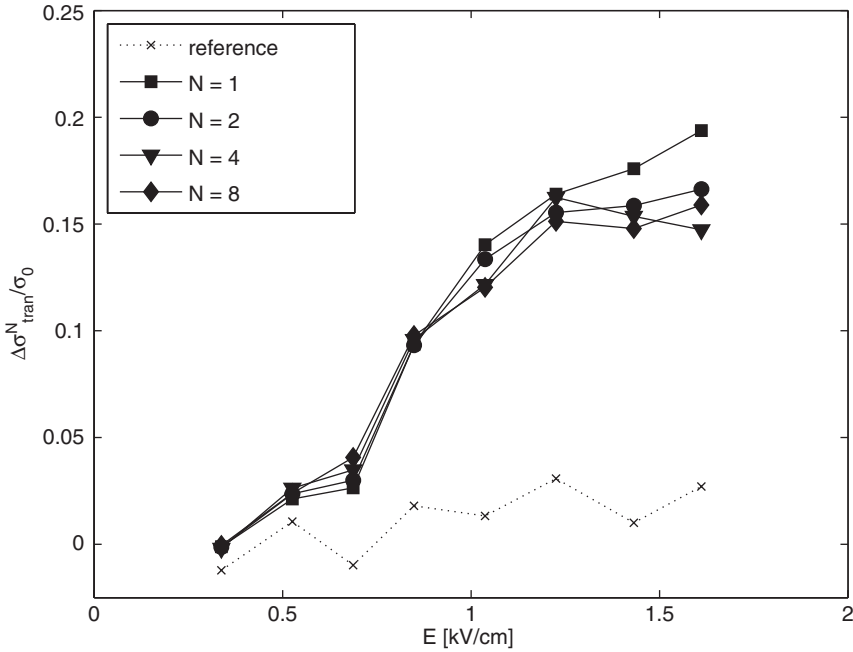
Figure 27 Transient conductivity changes during *N*-th pulse of the train of $8 \times 100\,\mu s$ pulses are shown. $\Delta\sigma^N_{\mathrm{tran}}$ is normalized to the initial conductivity. Solid line-cells in medium, dotted line-reference measurement on medium without cells during the first pulse.

Table 6 Calculation of conductivity inside the aqueous pore – values of used parameters.

N	e/kT	σ_{i}	U_{m}	R	D
0.15	$40\,\mathrm{V}^{-1}$	$0.5\,\mathrm{S/m}$	$900\,\mathrm{mV}$	$9.5\,\mu m$	$5\,\mathrm{nm}$
E	E_{c}	W_0	ρ	σ_{m}	D
$0.84\,\mathrm{kV/cm}$	$0.5\,\mathrm{kV/cm}$	2.5–5	0.22–0.57	1.4–$3.5 \times 10^{-5}\,\mathrm{S/m}$	$2.5 \times 10^{-5}\,\mathrm{cm}^2/\mathrm{s}$

The parameters are defined in Appendix B.1, the values used are presented in Table 6. For the membrane conductivity $\sigma_{\mathrm{m}} = [1.4 - 3.5] \times 10^{-5}$ and inserting values of parameters (see Table 6) we obtain for fraction of transient pores after $100\,\mathrm{s}$ pulse being $f_p = 10^{-5} - 10^{-4}$. Conductivity changes calculated theoretically taking into account the nonohmic behavior of the conductivity inside the pore using equation (46) are in good agreement with measured increase in conductivity during the pulses [125].

In Fig. 28, it is demonstrated that the conductivity changes relax almost to initial level in ten milliseconds (100 Hz) and after 1 s the following pulses have almost identical shape as the first pulse. This indicates that during electric pulses short–lived structural changes are formed which transiently increase ion permeation, but have very short lifetime after the pulses.
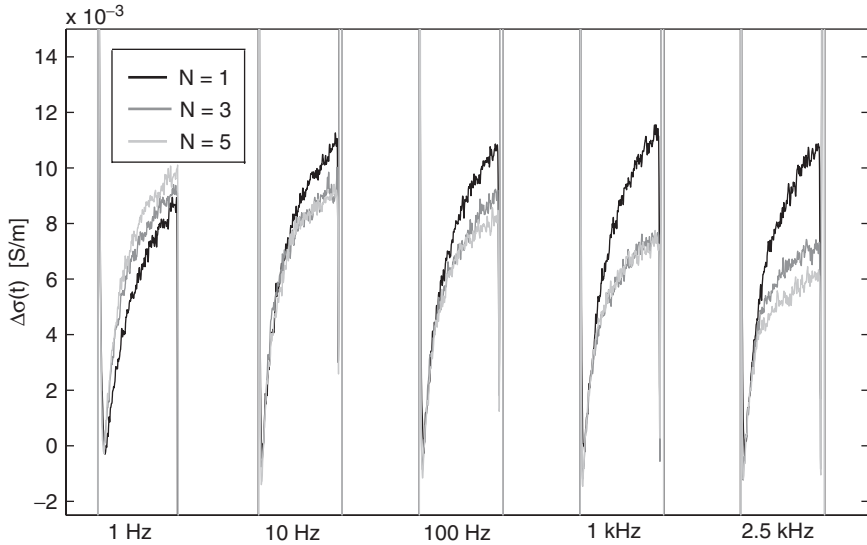
Figure 28 Effect of the repetition frequency on the conductivity changes. Pulses $8 \times 100\,\mu s$ with repetition frequencies from $1\,Hz$–$2.5\,kHz$ were used, $E = 0.84\,kV/cm$. The time-dependent conductivity changes $\Delta\sigma(t)$ of the first, third and the fifth pulse with respect to the first pulse (all initial levels are set to zero) are compared for different frequencies. Obtained from Ref. [125] with permission of Biophysical Society.

Altogether the conductivity measurements enable detection of short-lived permeable structures which are formed during the pulses. However since the conductivity drops to initial level in milliseconds after the pulses, these "pores" do not represent long-lived permeable structures which enable transport of molecules after the pulses.

4.4.3. Experimental studies of the effect of different parameters on molecular transport

The transport, which governs the uptake of molecules and leakage of cytoplasm contents, depends on experimental conditions, pulse parameters and the test molecule. The extensive studies of Teissié, Rols and colleagues, [30,96,120,138–141] examined the effect of different parameters (electric field strength, number of pulses, duration) on the extent of permeabilization uptake of exogenous molecules, cell survival, release of intracellular ATP and resealing. With these measurements it was shown that the critical parameter is the electric field strength and that the extent of permeabilization is governed by both duration and number of pulses. The authors define phenomenological electropermeabilization threshold E_p below which no transport is observed for given pulse parameters. However, they also define "limit" or real threshold E_s [30] which is the threshold below which no permeabilization occurs no matter how long the pulses are or how many are used. This threshold can be interpreted as the value of the electric field where critical transmembrane voltage is reached.

Two other extensive studies of electroporation *in vitro* were made [33,34], where authors studied uptake and viability for different electric field strength, duration, number of pulses and also different cell volume fractions. Data indicated that nei–ther electrical energy nor charge determines the extent of permeabilization and that the dependency is more complex. The results of these two studies also suggest that by increasing number and duration of pulses a certain "limit" threshold for perm–eabilization is reached, or in other words, the permeabilization curves start at the same electric field strength but the slope is electric field dependent. Even though some studies suggested [3] that pulse shape affects efficiency of electroporation our extensive study [142] of different pulse shapes showed that this is not crucial parameter.

The general observation on the resealing kinetics of cell electroporation is that resealing of the membrane lasts for minutes and is strongly dependent on the temperature. Together with the fact that a colloid–osmotic effect is also present it is obvious that complete resealing of the cell membrane is governed by slow bio–logical processes, which was shown that is ATP dependant.

4.4.4. Osmotic cell swelling

It was shown in several experiments that cells swell during electroporation [123–125,132]. Swelling of permeabilized cells is caused due to the difference in the permeabilities of ions and larger molecules (macromolecules) which results in an osmotic pressure that drives water into the cells and leads to cell swelling. The dynamics and the extent of cell swelling can be observed using imaging of cells during and after pulse application. The results of the measurements of the cell sizes during and after the pulses are shown in Fig. 29. The time constant of colloid osmotic swelling is few tens of seconds which is in agreement with the time constant for efflux of ions, which is between 10 and 20 s.
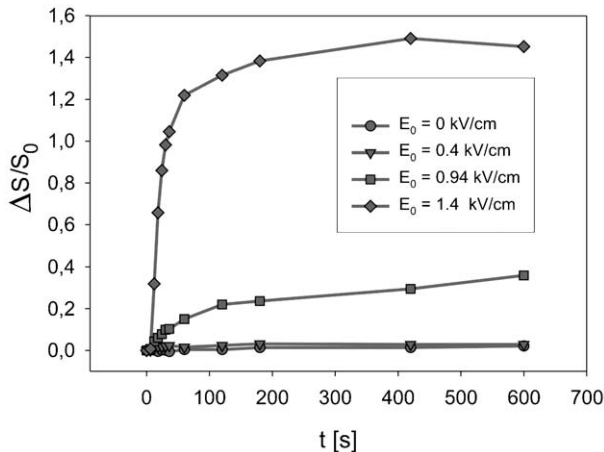
Figure 29   The effect of colloid–osmotic swelling – relative changes of the surface area $\Delta S/S_0$ of cells for different applied electric field strengths E_0 of the electric pulses ($8 \times 100\,\mu s$, $1\,Hz$) and control ($E_0 = 0\,kV/cm$), time $t = 0\,s$ – start of the first pulse, $t = 7\,s$ end of pulsation.

4.4.5. Quantification of ion diffusion and the fraction of long-lived pores

The process of ion transport during electroporation is similarly as transport of molecules governed mostly by diffusion. An increase in conductivity between the pulses due to ion efflux can be therefore used to determine the permeability coefficient and fraction of stable pores, which enable molecular transport which is crucial for successful application of electroporation.

The diffusion of ions is a slow process compared to the duration of the electric pulses thus we can assume that the major contribution to efflux of ions occurs without the presence of the electric field:

$$\frac{dc_e(t)}{dt} = -\frac{D\,S(E,N)}{d\,VF(1-F)}(c_e(t) - Fc_i(t)). \tag{47}$$

Definition of parameters and more detailed derivation is presented in Appendix B.2. The solution of above equation for $c_e(t)$ gives exponential rise to maximum, from which it follows that the conductivity between the pulses also increases as an exponential due to ion efflux. Form this it follows that the permeability coefficient k_N after the N-th pulse can be determined from the measured conductivity at N-th pulse ($\Delta\sigma_N$) and at $N+1$-th pulse ($\Delta\sigma_{N+1}$):

$$k_N = \frac{1}{\Delta t_N}\ln\left[1 - \frac{\Delta\sigma_N}{\Delta\sigma_{max}} \bigg/ 1 - \frac{\Delta\sigma_{N+1}}{\Delta\sigma_{max}}\right] \tag{48}$$

The permeability coefficient is directly proportional to the fraction of long-lived pores $-f_{per}$:

$$f_{per}^N \approx k_N \frac{dRF(1-F)}{3D'}, \quad D' = D\exp(-0.43w_0). \tag{49}$$

In Fig. 30 relative changes of the initial level of conductivity due to ion diffusion at the start of the N-th pulse $\Delta\sigma/\sigma_0 = (\sigma_0^N - \sigma_0)/\sigma_0$ for consecutive pulses are shown. Similarly as in Fig. 27 the initial level starts to increase for above the threshold $E > 0.5\,kV/cm$, which can be explained with the efflux of ions (mostly K^+ ions) from the cytoplasm through membrane pores. For higher electric fields ions efflux increases up to 1.6 kV depending also on the number of applied pulses. From measured $\Delta\sigma/\sigma_0 = (\sigma_0^N - \sigma_0)/\sigma_0$ using equation (48) we calculated permeability coefficients k_N which are proportional to fraction of long-lived pores (f_{per}). It can be seen (see Fig. 31) that k_N approximately linearly increases with number of pulses, and as expected increases also with the electric field strength.

4.4.6. The effect of electric field on long-lived pore formation and stabilization

Previously we have obtained the equation (see equation (43)) that determines how the electric field governs the area of the cell membrane, which is exposed to the above-critical transmembrane voltage U_c and has increased permeability: $S_c(E) = S_0\big((1 - E_c)/E\big)$. Furthermore, we can assume that pore formation in the area where $U > U_c$ is governed by the free energy of the pore, where the electrostatic term also includes the square of the electric field $\Delta W_e = aE^2$ [32,46]. Based on this we can assume that the most simplified equation, which describes the field
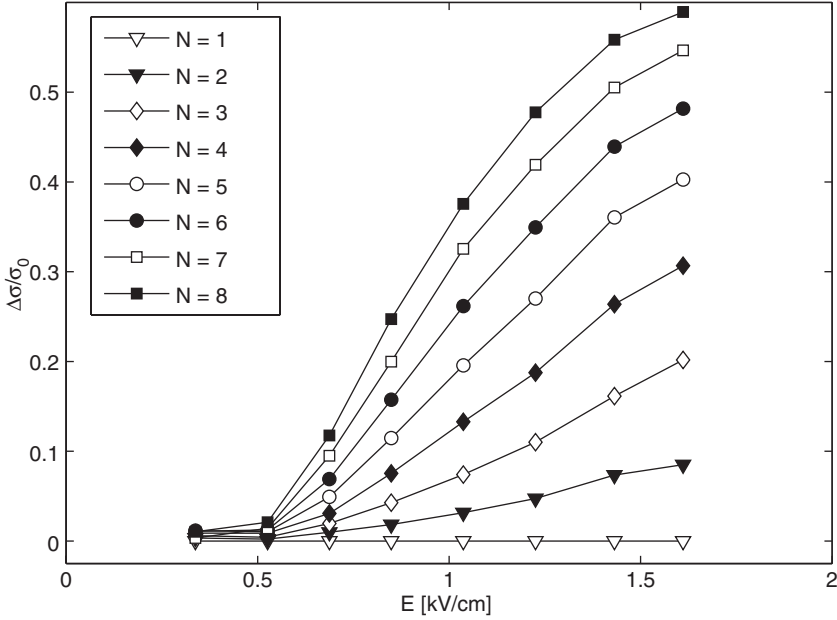
Figure 30 Relative conductivity changes between the pulses due to ion diffusion − $\Delta\sigma/\sigma_0 = (\sigma_0^N - \sigma_0)/\sigma_0$, where σ_0^N is the initial level at the start of the Nth pulse. $8 \times 100\,\mu s$ pulses were used with repetition frequency $1\,Hz$.
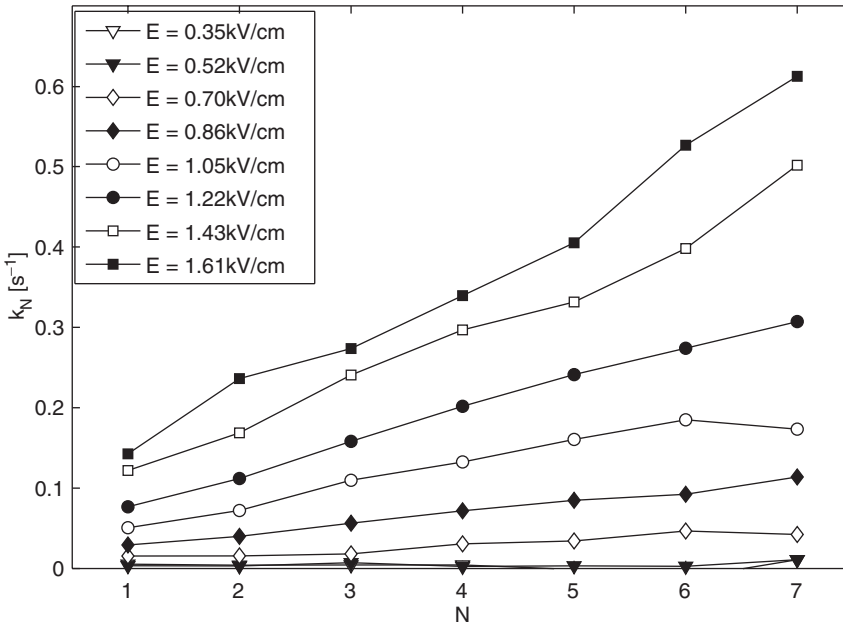
Figure 31 The permeability coefficients k_N for N pulses obtained after the N-th pulse calculated using equation (48) from the conductivity changes $\Delta\sigma/\sigma_0$ using $8 \times 100\,\mu s$ pulses. Obtained from Ref. [137] with permission of Elsevier.
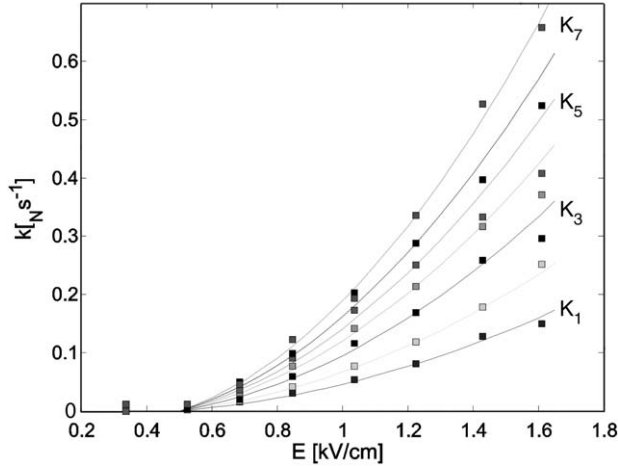
Figure 32 The permeability coefficients k_N for N pulses obtained after the N-th pulse calculated using equation (48) from the conductivity changes $\Delta\sigma/\sigma_0$ using 8×100 μs pulses. Comparison of the prediction of the model according to equation (50) (lines) and the measured permeability coefficients (symbols) is shown [137], with permission of Elsevier.

dependent permeability, can be written as [137]:

$$k_N(E) = C_N(1 - E_c/E)E^2. \tag{50}$$

where C_N are constants that depend on the size of the pores and their growth, and are thus dependent also on the number of pulses. The above equation takes into account the increase of the area of the cell exposed to the above critical voltage and the quadratic field dependence in the permeabilized region.

In Fig. 32 we compare the field dependence of the experimental permeability coefficient with the theoretical model. As expected, the permeability coefficient k_N and with this fraction of "transport" pores (see equation (48)) increases above the threshold electric field. More interestingly, this simple model (equation (50)) can very accurately describe the measured values, as can be seen in Fig. 32. This demonstrates that long-lived pore formation is governed also by the energy of the pores as well as by the number of pulses.

4.4.7. General experimental observations of cell electroporation

To summarize different phenomenological observations of cell electroporation (electropermeabilization)

- The state of transiently increased membrane conductivity indicates the existence of short-lived membrane structures which enable ion permeation. In the aqueous pores formation model of electroporation this corresponds to conductive hydrophilic pores [32]. An alternative explanation of these permeable structures was that they are structural mismatches in the lipid organization [143]. The membrane conductivity drops to the initial level in a range of a millisecond after

the pulses. This could be explained only with the existence of many small pores transient during the electric pulses, which close very rapidly (milliseconds) after the pulse. The number of these short-lived pores does not depend on the number of applied pulses but solely on the electric field strength and pulse duration.

- The state of increased permeability can last for tens of minutes after pulse application. Therefore, it is clear that in contrast to transient pores which reseal in milliseconds some pores are stabilized enabling transport across the membrane in minutes after the pulses. The quantification of ion efflux shows that in contrast to transient short-lived pores these stable pores are governed both by electric field strength as well as the number of pulses. The fraction of long-lived stable pores increases with higher electric field due to larger area of the cell membrane exposed to above critical voltage and due to higher energy which is available for pores formation. Moreover, each pulse increases the probability for the formation of the stable pores.
- The resealing of the cell membrane is a biologically active ATP-dependant process which strongly depends on the temperature and lasts from minutes to hours after pulse application. This clearly shows that long-lived pores are thermodynamically stable.

This and other observations lead to conclusion that the nature of long-lived "transport" pores is different than that of transient pores, which are present only during the pulses.

4.4.8. Possible theoretical explanations of long-lived pores

As shown in previous section there exist two types of pores (structural changes) of which nature, duration and number differs significantly. Hydrophilic pores are not stable after pulse application therefore some additional process must be involved in formation of stable pores. In Fig. 33 possible inter-relations between structural changes, conductivity changes and permeabilization (increased transport of molecules) are shown.

As shown in figure above the nature of long-lived pores and the relation between short-lived structural changes and long-lived is still not completely understood. In literature several explanations for the existence of these stable long-lived pores can be found. It was proposed that larger pores are formed by coalescence of smaller pores (defects) which travel in the membrane [144]. Some authors suggested that pores (defects) migrate along the membrane surface [32] and are grouped around inclusions. Altogether, there are no direct experimental observations which would confirm the hypothesis of a coalescence of pores.

There is general agreement that proteins are involved in stabilization of larger pores [32,46]. Authors speculated that cytoskeleton structure could act similarly to the macroscopic aperture of planar membrane experiments leading to rupture of limited portions of a cell membrane but not of the entire membrane [32]. Other authors suggested [139] that disintegration of the cytoskeleton network could affect electroporation where specific sites in the membrane would be more susceptible to
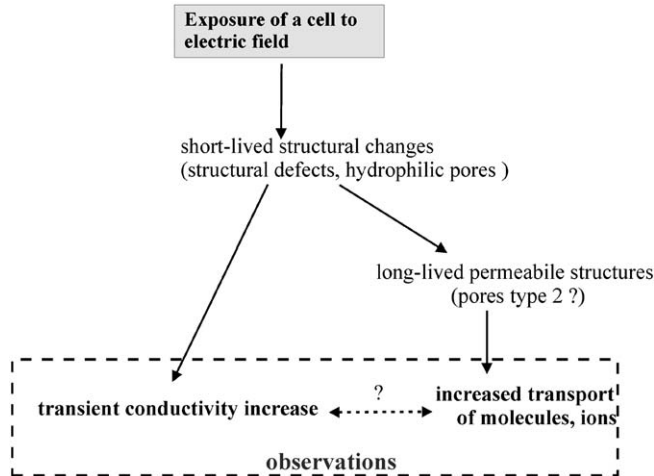
Figure 33 Possible inter-relations between structural changes, conductivity changes and permeabilization (increased transport of molecules).

pore formation. Some experiments suggest that only a few large pores contribute to increased permeability [145], whereas other suggests a contribution from a larger number of small defects due to the structural mismatches in the lipid membrane or due to structural discontinuities at borders between the domains. Recently it was also shown that anisotropic inclusions can stabilize pores in the membrane [146].

Altogether, there is still no definite explanation for the long-lived permeable structures in the cell membrane [99]. Whatever these structures are, they have long resealing times and are large enough to facilitate transport of larger molecules.

5. COMPARISON BETWEEN PLANAR LIPID BILAYERS AND CELL ELECTROPORATION

We have to stress that the described theories were developed for planar bilayer membranes which differ from cell membranes where membrane proteins and cytoskeleton are present. However, several experiments demonstrated that the structural changes probably occur in the lipid region of the cell membrane [29,32,147] and thus these theories can be applied to cell membranes as well.

Both in planar bilayer membranes and cell membranes the authors obtained a gradual increase of conductivity in high electric fields. The time interval preceding the irreversible breakdown and the rate of increase of conductivity are determined by the strength of the applied electric field [147]. The greatest observed difference is that the reversible electroporation in cells is much more common than in planar

bilayer membranes and that resealing of artificial bilayer membranes takes milliseconds whereas resealing of cells can last for several minutes. And specifically this long-lasting increased permeability of cell membrane is crucial for biotechnological and biomedical applications. This shows clearly that for a complete description of cell electroporation the role of the curvature, colloid osmotic swelling and specially cell structures, such as cytoskeleton, domains and membrane proteins have to be discussed and examined.

Altogether from theoretical model of aqueous pore formation can relatively good describe experimental observations on lipid bilayers: critical transmembrane voltage and stochastic nature of the process. However, up to now there is no theoretical description which could completely describe all observable phenomena present during cell electroporation and the underlying physical mechanism: the formation of structural changes in the membrane on a molecular level during the electric pulse, stochastic nature of electroporation, the observed dependency of molecular uptake on pulse duration and number of pulses, field strength, repetition frequency, the strong nonlinear transmembrane current-voltage characteristics with the critical transmembrane voltages between 0.2–1 V and the stability of "pores" after the pulses as well as the resealing dynamics.

Altogether, the model of an aqueous pore formation offers a plausible explanation for its stochastic nature and dependence on the pulse duration. The local minimum in the free energy could represent stable hydrophilic pores, which could explain the state of increase conductivity and permeability during the electric pulses. However, as it can be seen from Fig. 21, by using the realistic parameters a minimum in free energy is obtained only for very specific values of parameters usually suggesting that electroporation would immediately lead to irreversible electroporation. Thus as already discussed in the review of Weaver and Chizmadzhev, some additional processes/structures have to be included to obtain a realistic theoretical model of stable pores which could explain long-lived permeability of the cell membrane after electroporation. It is also clear that this theoretical description should incorporate proteins and cytoskeleton which can be crucial factors that enables pore stabilization and prevent breakdown of the cell membrane thus enabling the most important applications of cell electroporation: electrogene transfer and electrochemotherapy.

Strong support for the existence of pores was given recently by Marrink and colleagues in a molecular dynamics simulation of a lipid bilayer without [148] and in the presence [149] of an external electric field. Owing to thermal energy the lipid molecules constantly fluctuate and sometimes form short-lived states, with a structure similar to that of a small hydrophilic pore. By this, the assumption of the existence of small pores in the membrane before the application of the electric pulse is justified. The dynamic simulation in the presence of an external electric field [149] further showed existence of hydrophilic pores for the induced transmembrane voltage above 2.5 V, which is much higher than experimentally observed critical transmembrane voltage (0.2–1 V), however, these studies are important since they present calculations of the possible lipid states by taking into account forces on a molecular level. Future studies will probably enable building more realistic models.

▶ APPENDIX A

A.1. The Instability in the Hydrodynamic Model

In this model, the membrane is a layer of nonconductive liquid with permittivity ε_m and surface tension Γ. Its volume V is constant, while both its surface S and thickness d are variable, with initial values denoted by S_0 and d_0. The pressure exerted on the membrane by the transmembrane voltage U is given by

$$p_1 = \frac{\varepsilon_m U^2}{2d^2} \tag{A.1}$$

and is opposed by the pressure due to the increase of membrane surface, which is given by

$$p_2 = -\frac{\Gamma}{V} \int_{S_0}^{S} dS = -\frac{\Gamma(S - S_0)}{dS}. \tag{A.2}$$

Since in this model the volume is constant, $dS = d_0 S_0$, and we can write

$$p_2 = -\frac{\Gamma(S - S_0)}{d_0 S_0} = -\frac{\Gamma}{d_0}\left(\frac{S}{S_0} - 1\right) = -\frac{\Gamma}{d_0}\left(\frac{d_0}{d} - 1\right) = -\Gamma\left(\frac{1}{d} - \frac{1}{d_0}\right). \tag{A.3}$$

The equilibrium is obtained at a value of d at which $p_1 + p_2 = 0$:

$$\frac{\varepsilon_m U^2}{2d^2} - \Gamma\left(\frac{1}{d} - \frac{1}{d_0}\right) = 0 \tag{A.4}$$

We rewrite this expression as

$$\frac{1}{d_0}d^2 - d + \frac{U^2 \varepsilon_m}{2\Gamma} = 0. \tag{A.5}$$

This is a quadratic equation and thus has two solutions, but since at $U = 0$ the membrane thickness is by definition $d = d_0$, only one has a physical meaning, namely

$$d = \frac{d_0}{2}\left(1 + \sqrt{D}\right), \quad \text{where} \, D = 1 - \frac{2U^2 \varepsilon_m}{\Gamma d_0}. \tag{A.6}$$

Real solutions then exist only for $D \geq 0$, and the equilibrium is only reached at voltages below the critical value given by

$$U_c = \sqrt{\frac{\Gamma d_0}{2\varepsilon_m}}. \tag{A.7}$$

A.2. The Instability in the Elastic Model

We represent the membrane as an elastic layer with permittivity ε_m and elasticity module Y_m. We assume that the membrane surface S is constant, while its volume V and its thickness d are variable, with initial values V_0 and d_0. The pressure caused

by the voltage U is again

$$p_1 = \frac{\varepsilon_{\mathrm{m}} U^2}{2d^2} \tag{A.8}$$

and is opposed by the pressure due to the compression of the membrane volume,

$$p_2 = \int_{V_0}^{V} \frac{Y(V)}{V} \, \mathrm{d}V. \tag{A.9}$$

Assuming that Y does not vary with the deformation, we get

$$p_2 = Y \int_{V_0}^{V} \frac{\mathrm{d}V}{V} = -Y \ln \frac{V_0}{V} = -Y \left(\ln \frac{d_0}{d} + \ln \frac{S_0}{S} \right). \tag{A.10}$$

Since we assume a constant surface, $S = S_0$, the second logarithm is zero, and we have

$$p_2 = -Y \ln \frac{d_0}{d}. \tag{A.11}$$

The equilibrium is obtained at a value of d which gives $p_1 + p_2 = 0$:

$$\frac{\varepsilon_{\mathrm{m}} U^2}{2d^2} - Y \ln \frac{d_0}{d} = 0 \tag{A.12}$$

which we rewrite as

$$\frac{\varepsilon_{\mathrm{m}} U^2}{Y d^2} = \ln \frac{d_0^2}{d^2}. \tag{A.13}$$

Let $\chi = d_0^2/d^2$; then

$$K\chi = \ln \chi, \quad \text{where} K = \frac{\varepsilon_{\mathrm{m}} U^2}{Y d_0^2}. \tag{A.14}$$

This equation is not solvable analytically, but it is easily verified that real solutions exist only for $K \leq 1/e$. The equilibrium is thus only reached below the critical voltage given by

$$U_{\mathrm{c}} = d_0 \sqrt{\frac{Y}{e \varepsilon_{\mathrm{m}}}} \approx 0.61 d_0 \sqrt{\frac{Y}{\varepsilon_{\mathrm{m}}}}. \tag{A.15}$$

A.3. The Instability in the Hydroelastic Model

We assign to the membrane a permittivity ε_{m}, surface tension Γ and elasticity module Y, and we assume that the volume V, surface S and thickness d of the membrane are all variable, with initial values of the latter two denoted by S_0 and d_0. The pressure generated by the transmembrane voltage is opposed by the pressures due to the membrane surface tension and elasticity (see Appendices A.1 and A.2),

with the equilibrium given by

$$\frac{\varepsilon_m U^2}{2d^2} - \frac{\Gamma(S - S_0)}{dS} - Y \ln \frac{d_0}{d} - Y \ln \frac{S_0}{S} = 0. \tag{A.16}$$

We rewrite this expression as

$$\frac{\varepsilon_m U^2}{2Yd^2} + \frac{\Gamma S_0}{YdS} - \frac{\Gamma}{Yd} = \ln \frac{d_0}{d} + \ln \frac{S_0}{S} \tag{A.17}$$

and substitute $\psi = d_0/d$, $\xi = S_0/S$, to get

$$K_1 \psi^2 - K_2 \psi (1 - \xi) = \ln \psi + \ln \xi \tag{A.18}$$

where $K_1 = \varepsilon_m U^2 / 2Yd_0^2$ and $K_2 = \Gamma/Yd_0$. While in the direction perpendicular to the membrane surface, the pressures due to the elasticity and surface tension are co-oriented, in the direction parallel to the membrane they oppose each other, so in the equilibrium

$$\frac{\Gamma(S - S_0)}{dS} - Y \ln \frac{d_0}{d} - Y \ln \frac{S_0}{S} = 0. \tag{A.19}$$

With the same notation as above, this gives

$$K_2 \psi (1 - \xi) = \ln \psi + \ln \xi. \tag{A.20}$$

Subtracting this equation from the first equilibrium equation, we get

$$K_1 \psi^2 - 2K_2 \psi (1 - \xi) = 0 \tag{A.21}$$

and hence

$$1 - \xi = \frac{K_1}{2K_2} \psi. \tag{A.22}$$

Inserting this result into the second equilibrium equation, we finally get

$$\frac{K_1 \psi^2}{2} = \ln \psi + \ln \left(1 - \frac{K_1}{2K_2} \psi \right). \tag{A.23}$$

This equation does not have a solution expressible as an elementary function, and to determine U_c, we insert actual parameter values and calculate ψ numerically for increasing values of U, until we reach the point $U = U_c$ for which no real solutions exist.

A.4. The Instability in the Viscohydroelastic Model

In a membrane with permittivity ε_m, surface tension Γ, elasticity module Y and viscosity μ, discontinuities occur after the transmembrane voltage U has been present for the critical duration given by

$$\tau_c = \frac{24\mu}{2\varepsilon_m U^2 k^2 - 8Y - \Gamma d_0^3 k^4} \tag{A.24}$$

where k is the wave number (the reciprocal of the length of the ripples on the membrane). Note that at low values of U, we would obtain a negative value of τ_c, which is physically meaningless; this means that the membrane is stable, and the discontinuities cannot occur at any τ_c. If the ripples can form freely (i.e. if there are no fixed points on the membrane), for a given U the wave number takes a value at which the value of τ_c is minimal

$$\frac{d\tau_c}{dk} = \frac{96\mu(\varepsilon_m U^2 k - \Gamma d_0^3 k^3)}{(2\varepsilon_m U^2 k^2 - 8Y - \Gamma d_0^3 k^4)^2}. \tag{A.25}$$

The solution $k = 0$ is meaningless as it would imply that the ripples are infinitely large, so we have

$$k^2 = \frac{\varepsilon_m U^2}{\Gamma d_0^3}. \tag{A.26}$$

Inserting this value into the expression for the critical duration, we get

$$\tau_c = \frac{24\mu}{\frac{\varepsilon_m^2 U^4}{\Gamma d_0^3} - 8Y}. \tag{A.27}$$

This expression takes a positive value only at voltages above the critical amplitude given by

$$U_c = \sqrt[4]{\frac{8\Gamma Y d_0^3}{\varepsilon_m^2}} \tag{A.28}$$

and the discontinuities occur if a voltage $U > U_c$ lasts longer than the critical duration at this voltage (see Fig. 14).

A.5. The Energy of a Hydrophilic Pore

At a distance ρ from the center of a cylindrical pore with a radius r, the strength of hydrophobic interaction is given by

$$\eta(\rho) = \eta_0 \frac{I_0(\rho/\lambda)}{I_0(r/\lambda)} \tag{A.29}$$

where η_0 is the value of $\eta(\rho)$ directly at the surface, λ the characteristic length of hydrophobic interaction and I_k the modified Bessel function of k-th order. Simultaneously, the total energy of this interaction is described as

$$W = 2\pi d \int_0^r \left[\eta^2(\rho) + \lambda^2 \left(\frac{d\eta(\rho)}{d\rho} \right)^2 \right] \rho \, d\rho \tag{A.30}$$

where d is the height of the pore (the thickness of the membrane). By joining these expressions, we obtain

$$W = 2\pi dr \lambda \eta_0^2 \frac{I_1(r/\lambda)}{I_0(r/\lambda)}. \tag{A.31}$$

At $r \gg \lambda$, the ratio of the two Bessel functions approaches 1, and W is proportional to the pore surface $S = 2\pi rd$,

$$W = S \lambda \eta_0^2 \tag{A.32}$$

which shows that $\lambda \eta_0^2$ corresponds to the surface tension Γ_h at the interface of the hydrophobic surface and water. Since Γ_h is measurable, it is then sensible to rewrite the energy of the pore as

$$W = 2\pi dr \Gamma_h \frac{I_1(r/\lambda)}{I_0(r/\lambda)}. \tag{A.33}$$

APPENDIX B

B.1. Calculation of the Fraction of Surface Area of Transient Pores

Here, we present the estimation of the fraction of the surface area of pores in the cell membrane from the increased membrane conductivity (similar derivation was first presented by Hibino [84]). We assume that the specific conductance of the permeabilized area of a cell is approximately the sum of the conductance of N_p pores having radius r_p

$$G_p = N_p \pi r_p^2 \frac{\sigma_{por}}{d} = S_{por} \frac{\sigma_{por}}{d} \tag{B.1}$$

where we neglect the very small conductance of nonpermeabilized cell membrane and S_{por} represents the surface of all conducting pores. On the other hand, this conductance is equal to the average membrane conductance of the permeabilized area as obtained from our measurement and from the theoretical model $G_p = G_{meas}$, thus

$$S_{por} \frac{\sigma_{por}}{d} = S_c \frac{\sigma_m}{d} \tag{B.2}$$

where S_c represents the total permeabilized surface of one cell (the area exposed to above-threshold transmembrane voltage $- S_c = S_0 \left((1 - E_c)/E \right)$ and σ_m the average membrane conductivity of permeabilized area as defined in the theoretical model. From this it follows that the fraction of pores is

$$f_p = \frac{S_{por}}{S_0} = \frac{S_c \sigma_m}{S_0 \sigma_{por}} \approx \frac{\left((1 - E_c)/E \right) \sigma_m}{\sigma_{por}} \approx \frac{\left((1 - E_c)/E \right) \sigma_m}{\rho \sigma_{0por}} \tag{B.3}$$

where parameter ρ takes into account that conductivity inside the pores differs from bulk. Namely, conductance of the pore in an 1:1 electrolyte is given by [46]

$$G_{por} = G_0 \frac{\exp(\beta U_m) - 1}{\frac{\beta U_m}{d} \int_0^d \exp\left[\beta U_m \frac{d-x}{d} + w(x)\right] dx} = G_0 \rho, \quad G_0 = N_p \pi r_p^2 \frac{\sigma_{0por}}{d} \quad (B.4)$$

where $\beta = e/kT$ and $w(x) = W(x)/kT$ where e is the electron charge, U_m the transmembrane voltage and $W(x)$ the energy of an ion inside the pore due to the interactions of the ion with the pore walls [46,150]. Parameter ρ is a scaling factor, which reduces the conductivity of the ions inside the pores (σ_{por}), compared to the bulk approximation $\sigma_{0por} \approx (\sigma_e + \sigma_i)/2$ in the limit of very large pores when interactions are negligible. For a trapezoid shape of $w(x)$ we obtain from equation (B.4) that when the transmembrane voltage is small $n\beta U_m \ll w_0$:

$$\rho = \exp[-0.43(w_0 - n\beta U_m)] \quad (B.5)$$

which is true for physiological conditions where resting transmembrane voltage is between 50 and 100 mV. When we apply external electric field typical for electroporation the transmembrane voltage is large and thus we can use approximation $n\beta U_m \gg w_0 (U_E \gg 25 \text{ mV})$ and we obtain

$$\rho = \frac{1}{\left(1 + \frac{n\beta U_m}{w_0 - n\beta U_m}\right) \exp(w_0 - n\beta U_m) - \frac{n\beta U_m}{w_0 - n\beta U_m}} \quad (B.6)$$

where n is the relative size of the entrance region of the pore and was estimated to be approximately 0.15 [46]. W_0 is the energy of an ion inside center of a pore and was estimated to be few kT [46,151,152].

B.2. Quantification of Ion Diffusion and Long-Lived Pores

Here we analyze theoretically the changes of conductivity on the time scale of seconds, where diffusion of ions dominates. The transport of ions through the membrane is governed by Nernst–Planck equation:

$$\frac{dn_e(x, t)}{dt} = -DS \frac{dc(x, t)}{dx} - \frac{zF}{RT} DSc(x, t) \frac{d\Psi(x, t)}{dx} \quad (B.7)$$

where n_e is the number of moles in the external medium, D the diffusion constant ($\approx 2 \times 10^{-5} \text{cm}^2/\text{s}$), c the molar concentration, S the total transport surface $S = N_c S_{por}$ of N_c permeabilized cells and Ψ the electric potential. In general D and S depend on time, pulse duration, electric field strength and number of pulses. Here we will first analyze the ion efflux after the N pulses so only S will depend on N, and D will be constant. The diffusion of ions is a slow process compared to the duration of the electric pulses thus we can assume that the major contribution to efflux of ions occurs without the presence of the electric field. When there is no external electric field present $\Delta\Psi$ is small since only the imbalance of the electric charges due to concentration gradient contributes. Therefore the second term in equation (B.7) can be neglected. By replacing the concentration gradient with $(c_e - c_i)/d$ and by taking into account that the sum of ions inside and outside

remains constant, the equation further simplifies:

$$\frac{dc_e(t)}{dt} = -\frac{DS(E,N)}{dVF(1-F)}\left(c_e(t) - Fc_i^0\right) \tag{B.8}$$

where c_i^0 is the initial internal concentration of K^+ ions, V_e represent the external volume and function $S(E,N)$ describes the field dependent surface of pores. If we further neglect the volume fraction changes and assume that S is approximately constant, we obtain that the solution of the above equation is an exponential increase to maximum $c_e^{max} = Fc_i^0$

$$c_e(t) = c_e^{max}\left[1 - \exp\left(-\frac{t}{\tau}\right)\right] \tag{B.9}$$

with a time constant τ and permeability coefficient k being dependent on the fraction of transport pores f_{per}:

$$\tau = \frac{1}{f_E}\frac{3D}{dRF(1-F)}, \quad k = 1/\tau. \tag{B.10}$$

By measuring current and voltage during the train of successive pulses we obtain the change of the initial level of the conductivity, i.e. conductivity increase due to the ion efflux. Taking into account that the permeability coefficient depends on the number of pulses we can express the measured change of conductivity with [137]:

$$\frac{\Delta\sigma(t)}{\sigma_0} = \sum_N A_N\left[1 - \exp(-k_N t)\right]. \tag{B.11}$$

From this it follows that the permeability coefficient after the N-th pulse can be determined from the measured conductivity at N-th pulse ($\Delta\sigma_N$) and at N+1-th pulse ($\Delta\sigma_{N+1}$):

$$k_N = \frac{1}{\Delta t_N}\ln\left[1 - \frac{\Delta\sigma_N}{\Delta\sigma_{max}}\bigg/1 - \frac{\Delta\sigma_{N+1}}{\Delta\sigma_{max}}\right] \tag{B.12}$$

where Δt_N is the time difference between N-th and N+1-th pulse and $\Delta\sigma_{max}$ is the maximum value of the conductivity, i.e. the saturation point when the concentrations inside and outside the cell are equal. From the permeability coefficient k_N the fraction of "transport" pores can be estimated using equation (B.10):

$$f_E^N \approx k_N\frac{dRF(1-F)}{3D'}, \quad D' = D\exp(-0.43w_0) \tag{B.13}$$

where we take into account that the effective diffusion constant D' of K^+ ions inside the pore differs from that in the bulk [46,151,152].

REFERENCES

[1] R.B. Gennis, Biomembranes, Molecular Structure and Function, Springer, New York, 1989.
[2] E. Neumann, A. Sowers, C. Jordan, Electroporation and Electrofusion in Cell Biology, Plenum, New York, 1989.

[3] D.C. Chang, B.M. Chassey, J.A. Saunders, A.E. Sowers, Guide to Electroporation and Elect-rofusion, Academic Press, New York, 1992.

[4] R. Stampfli, Reversible electrical breakdown of the excitable membrane of a Ranvier node, Ann. Acad. Brasil. Ciens. 30 (1958) 57–63.

[5] A.J.H. Sale, A. Hamilton, Effects of high electric fields on microorganisms: I. Killing of bacteria and yeasts, Biochem. Biophys. Acta 148 (1967) 781–788.

[6] E. Neumann, K. Rosenheck, Permeability changes induced by electric impulses in vesicular membranes, J. Membr. Biol. 10 (1972) 279–290.

[7] E. Neumann, M.S. Ridder, Y. Wang, P.H. Hofschneider, Gene transfer into mouse lyoma cells by electroporation in high electric fields 1 (1982) 841–845.

[8] M. Okino, H. Mohri, Effects of high-voltage electrical impulse and an anticancer drug on in vivo growing tumors, Jpn. J. Cancer Res. 78 (1987) 1319–1321.

[9] L.M. Mir, H. Banoun, C. Paoletti, Introduction of definite amounts of nonpermeant molecules into living cells after electropermeabilization: direct access to the cytosol, Exp. Cell Res. 175 (1988) 15–25.

[10] D. Miklavčič, M. Puc, Electroporation, Wiley Encyclopedia of Biomedical Engineering, Wiley, New York, 2006.

[11] J. Teissié, N. Eynard, M.C. Vernhes, A. Benichou, V. Ganeva, B. Galutzov, P.A. Cabanes, Recent biotechnological developments of electropulsation. A prospective review, Bioelectro-chemistry 55 (2002) 107–112.

[12] C.N. Haas, D.N. Aturaliye, Kinetics of electroporationassisted chlorination of giardia muris, Water Res. 33 (1999) 1761–1766.

[13] N.J. Rowan, S.J. MacGregor, J.G. Anderson, R.A. Fouracre, O. Farish, Pulsed electric field inactivation of diarrhoeagenic *Bacillus cereus* through irreversible electroporation, Lett. Appl. Microbiol. 31 (2000) 110–114.

[14] L.M. Mir, Therapeutic perspectives of in vivo cell electropermeabilization, Bioelectrochemistry 53 (2001) 1–10.

[15] J. Gehl, Review: electroporation: theory and methods, perspectives for drug delivery, gene therapy and research, Acta Physiol. Scand. 177 (2003) 437–447.

[16] L.M. Mir, S. Orlowski, J. Belehradek, J. Teissié, M.P. Rols, G. Serša, D. Miklavčič, R. Gilbert, R. Heller, Biomedical applications of electric pulses with special emphases on antitumor electrochemotherapy, Bioelectrochem. Bioenerg. 38 (1995) 203–207.

[17] G. Serša, B. Štabuc, M. Čemažar, B. Jančar, D. Miklavčič, Z. Rudolf, Electrochemotherapy with cisplatin: potentiation of local cisplatin antitumor effectiveness by application of electric pulses in cancer patients, Eur. J. Cancer 34 (1998) 1213–1218.

[18] R. Heller, R. Gilbert, M.J. Jaroszeski, Clinical application of electrochemotherapy, Adv. Drug Deliv. Rev. 35 (1999) 119–129.

[19] Y. Mouneimne, P.F. Tosi, R. Barhoumi, C. Nicolau, Electroinsertion of full length recom-binant CD4 into red blood cell membrane, Biochim. Biophys. Acta 1027 (1990) 53–58.

[20] S. Raffy, J. Teissié, Electroinsertion of glycophorin A in interdigitation-fusion giant unilamellar lipid vesicles, J. Biol. Chem. 272 (1997) 25524–25530.

[21] I.G. Abidor, A.E. Sowers, Kinetics and mechanism of cell membrane electrofusion, Biophys. J. 61 (1992) 1557–1569.

[22] A.E. Sowers, Membrane electrofusion: a paradigm for study of membrane fusion mechanisms, Methods Enzymol. 220 (1993) 196–211.

[23] H. Mekid, L.M. Mir, In vivo cell electrofusion, Biochim. Biophys. Acta 1524 (2000) 118–130.

[24] T.H. Scott-Taylor, R. Pettengell, I. Clarke, G. Stuhler, M.C. La Barthe, P. Walden, A.G. Dalgleish, Human tumour and dendritic cell hybrids generated by electrofusion: potential for cancer vaccines, Biochim. Biophys. Acta 1500 (2000) 265–267.

[25] E. Schmidt, U. Leinfelder, P. Gessner, D. Zillikens, E.B. Brocker, U. Zimmermann, CD19+ B lymphocytes are the major source of human antibody-secreting hybridomas generated by electrofusion, J. Immunol. Methods 255 (2001) 93–102.

[26] M.R. Prausnitz, V.G. Bose, R. Langer, J.C. Weaver, Electroporation of mammalian skin: a mechanism to enhance transdermal drug delivery, Proc. Natl. Acad. Sci. U.S.A. 90 (1993) 10504–10508.

[27] R. Vanbever, N. Lecouturier, V. Preat, Transdermal delivery of metoprolol by electroporation, Pharmacol. Res. 11 (1994) 1657–1662.

[28] T.E. Zewert, U. Pliquett, R. Langer, J.C. Weaver, Transport of DNA antisense oligonucleotides across human skin by electroporation, Biochem. Biophys. Res. Commun. 212 (1995) 286–292.

[29] U. Zimmermann, Electric field-mediated fusion and related electrical phenomena, Biochim. Biophys. Acta 694 (1982) 227–277.

[30] M.P. Rols, J. Teissié, Electropermeabilization of mammalian cells. quantitative analysis of the phenomenon, Biophys. J. 58 (1990) 1089–1098.

[31] T.Y. Tsong, Electroporation of cell membranes, Biophys. J. 60 (1991) 297–306.

[32] J.C. Weaver, Y.A. Chizmadzhev, Theory of electroporation: a review, Bioelectrochem. Bioenerg. 41 (1996) 135–160.

[33] P.J. Canatella, J.F. Karr, J.A. Petros, M.R. Prausnitz., Quantitative study of electroporation-mediated molecular uptake and cell viability, Biophys. J. 80 (2001) 755–764.

[34] A. Maček-Lebar, D. Miklavčič, Cell electropermeabilization to small molecules in vitro: control by pulse parameters, Radiol. Oncol. 35 (2001) 193–202.

[35] D. Miklavčič, T. Kotnik, Electroporation for electrochemotherapy and gene therapy, in: P.J. Rosch, M.S. Markov (Eds.), Bioelectromagnetic Medicine, Marcel Dekker, New York, 2004, pp. 637–656.

[36] M. Smeyers, M. Leonetti, E. Goormaghtigh, F. Homble, Structure and function of plant membrane ion channels reconstituted in planar lipid bilayers, in: H.T. Tien, A. Ottova–Leitmannova (Eds.), Planar Lipid Bilayers (BLMs) and Their Applications, Elsevier, New York, 2003, pp. 449–478.

[37] G.C. Troiano, L. Tung, V. Sharma, K.J. Stebe, The reduction in electroporation voltages by the addition of surfactant to planar lipid bilayer, Biophys. J. 75 (1998) 880–888.

[38] V. Sharma, K. Uma Maheswari, J.C. Murphy, L. Tung, Poloxamer 188 decreases susceptibility of artificial lipid membranes to electroporation, Biophys. J. 71 (1996) 3229–3241.

[39] W. Meier, A. Graff, A. Diederich, M. Winterhalter, Stabilization of planar lipid membranes: a stratified layer approach, Phys. Chem. Chem. Phys. 2 (2000) 4559–4562.

[40] A. Diederich, G. Bahr, M. Winterhalter, Influence of surface charges on the rapture of black lipid membranes, Phys. Rev., E 58 (1998) 4883–4889.

[41] R. Benz, K. Janko, Voltage-induced capacitance relaxation of lipid bilayer membranes; effects on membrane composition, Biochim. Biophys. Acta 455 (1976) 721–738.

[42] J. Vargas, J.M. Alarcon, E. Rojas, Displacement currents associated with the insertion of Alzheimer disease amyloid (beta)-peptide into planar bilayer membranes, Biophys. J. 79 (2000) 934–944.

[43] C. Wilhelm, M. Winterhalter, U. Zimmermann, R. Benz, Kinetics o pore size during irreversible electrical breakdown of lipid bilayer membranes, Biophys. J. 64 (1993) 121–128.

[44] R. Benz, F. Beckers, U. Zimmermann, Reversible electrical breakdown of lipid bilayer membranes: a charge-pulse relaxation study, J. Membr. Biol. 48 (1979) 181–204.

[45] K.C. Melikov, V.A. Frolov, A. Shcherbakov, A.V. Samsonov, Y.A. Chizmadzhev, L.V. Chernomordik, Voltage-induced nonconductive pre-pores and metastable single pores in unmodified planar lipid bilayer, Biophys. J. 80 (2001) 1829–1836.

[46] R.W. Glaser, S.L. Leikin, L.V. Chernomordik, V.F. Pastushenko, A.I. Sokirko, Reversible electrical breakdown of lipid bilayers: formation and evolution of pores, Biochim. Biophys. Acta 940 (1988) 275–287.

[47] I.G. Abidor, V.B. Arakelyan, L.V. Chernomordik, Y.A. Chizmadzhev, V.F. Pastushenko, M.R. Tarasevich, Electric breakdown of bilayer membranes: I. The main experimental facts and their qualitative discussion, Bioelectrochem. Bioenerg. 6 (1979) 37–52.

[48] A.N. Chanturiya, Detection of transient capacitance increase associated with channel formation in lipid bilayers, Biochim. Biophys. Acta 1026 (1990) 248–250.

[49] S. Kalinowski, Z. Figaszewski, A new system for bilayer lipid membrane capacitance measurements: method apparatus and applications, Biochim. Biophys. Acta 1112 (1992) 57–66.

[50] S. Koronkiewicz, S. Kalinowski, K. Bryl, Programmable chronopotentiometry as a tool for the study of electroporation and resealing of pores in bilayer lipid membranes, Biochim. Biophys. Acta 1561 (2002) 222–229.

[51] A. Ridi, E. Scalas, M. Robello, A. Gliozzi, Linear response of a fluctuating lipid bilayer, Thin Solid Films 327–329 (1998) 796–799.

[52] M. Robello, A. Gliozzi, Conductance transition induced by an electric field in lipid bilayers, Biochim. Biophys. Acta 982 (1989) 173–176.

[53] A. Ridi, E. Scalas, A. Gliozzi, Noise measurements in bilayer lipid membranes during electroporation, EPJ E 2 (2000) 161–168.

[54] E. Scalas, A. Ridi, M. Robello, A. Gliozzi, Flicker noise in bilayer lipid membranes, Europhys. Lett. 43 (1998) 101–105.

[55] I. Genco, A. Gliozzi, A. Relini, M. Robello, E. Scalas, Electroporation in symmetric and asymmetric membranes, Biochim. Biophys. Acta 1149 (1993) 10–18.

[56] E. Pescio, A. Ridi, A. Gliozzi, A picoampere current generator for membrane electroporation, Rev. Sci. Instrum. 71 (2000) 1740–1744.

[57] M. Robello, M. Fresia, L. Maga, A. Grasso, S. Ciani, Permeation of divalent cations trough (alpha)-latrotoxin channels in lipid bilayers: steady-state current-voltage relationship, J. Membr. Biol. 95 (1987) 55–62.

[58] S. Kalinowski, Z. Figaszewski, A four-electrode potentiostat-galvanostat for studies of bilayer lipid membranes, Meas. Sci. Technol. 6 (1995) 1050–1055.

[59] S. Micelli, E. Gallucci, V. Ricciarelli, Studies of mitochondrial porin incorporation parameters and voltage-gated mechanism with different black lipid membranes, Bioelectrochemistry 52 (2000) 63–75.

[60] P. Kramar, D. Miklavčič, A. Maček-Lebar, Determination of the lipid bilayer breakdown voltage by means of a linear rising signal, Bioelectrochemistry 70 (2007) 23–27.

[61] A. Blume, Lipids, in: D. Waltz, J. Teissié, G. Milazzo (Eds.), Bioelectrochemistry of membranes, Birkhauser, Basel-Boston-Berlin, 2004, pp. 24–61.

[62] Y. Hanyu, T. Yamada, G. Matsumoto, Simultaneous measurement of spectroscopic and physiological signals from a planar bilayer system: detecting voltage-dependent movement of a membrane-incorporated peptide, Biochemistry 37 (1998) 15376–15382.

[63] H. Yamaguchi, H. Nakanishi, Characterization of the preparation process and photochemical control of electrical properties of bilayer lipid membranes containing azobenzene chromophores, Biochim. Biophys. Acta 1148 (1993) 179–184.

[64] T.F. Eibert, M. Alaydrus, F. Wiczewski, V.W. Hansen, Electromagnetic and thermal analysis for lipid bilayer membranes exposed to RF fields, IEEE Trans. Biomed. Eng. 46 (1999) 1013–1021.

[65] N. Montal, P. Mueller, Formation of bimolecular membranes from lipid monolayers and a study of their electrical properties, Proc. Natl. Acad. Sci. U.S.A. 69 (1972) 3561–3566.

[66] A. Maček Lebar, G.C. Troiano, L. Tung, D. Miklavcic, Inter-pulse interval between rectangular voltage pulses affects electroporation threshold of artificial lipid bilayers, IEEE Trans. Nanobioscience 1 (2002) 116–120.

[67] E. Evans, V. Heinrich, F. Ludwig, W. Rawicz, Dynamic tension spectroscopy and strength of biomembranes, Biophys. J. 85 (2003) 2342–2350.

[68] E. Gallucci, S. Micelli, G. Monticelli, Pore formation in lipid bilayer membranes made of phosphatidylinositol and oxidized cholesterol followed by means of alternating current, Biophys. J. 71 (1996) 824–831.

[69] L.V. Chernomordik, S.I. Sukharev, I.G. Abidor, Yu.A. Chizmadzhev, Breakdown of lipid bilayer membranes in an electric field, Biochim. Biophys. Acta 736 (1983) 203–213.

[70] S. Kalinowski, G. Ibron, K. Bryl, Z. Figaszewski, Chronopotentiometric studies of electroporation of bilayer lipid membranes, Biochim. Biophys. Acta 1396 (1998) 204–212.

[71] P.R.C. Gascoyne, R. Pethig, J.P.H. Burt, F.F. Becker, Membrane changes accompanying the induced differentiation of Friend murine erythroleukemia cells studied by dielectrophoresis, Biochim. Biophys. Acta 1146 (1993) 119–126.

[72] I.P. Sugár, A theory of the electric field-induced phase transition of phospholipid bilayers, Biochim. Biophys. Acta 556 (1979) 72–85.

[73] D.S. Dimitrov, R.K. Jain, Membrane stability, Biochim. Biophys. Acta 779 (1984) 437–468.

[74] C.M. Harris, D.B. Kell, The radio-frequency dielectric properties of yeast cells measured with a rapid automated, frequency-domain dielectric spectrometer, Bioelectrochem. Bioenerg. 11 (1983) 15–28.

[75] R. Hlzel, I. Lamprecht, Dielectric properties of yeast cells as determined by electrorotation, Biochim. Biophys. Acta 1104 (1992) 195–200.

[76] F.W. Sunderman, Measurement of serum total base, Am. J. Clin. Pathol. 15 (1945) 219–222.

[77] K. Nrtemann, J. Hilland, U. Kaatze, Dielectric properties of aqueous NaCl solutions at microwave frequencies, J. Phys. Chem. A 101 (1997) 6864–6869.

[78] D.H. Michael, M.E. O'Neill, Electrohydrodynamic instability in plane layers of fluid, J. Fluid Mech. 41 (1970) 571–580.

[79] G.I. Taylor, D.H. Michael, On making holes in a sheet of fluid, J. Fluid Mech. 58 (1973) 625–639.

[80] J.M. Crowley, Electrical breakdown of bimolecular lipid membranes as an electro-mechanical instability, Biophys. J. 13 (1973) 711–724.

[81] C. Maldarelli, R.K. Jain, I.B. Ivanov, E. Rckenstein, Stability of symmetric and unsymmetric, thin liquid films to short and long wavelength perturbations, J. Colloid Interface Sci. 78 (1980) 118–143.

[82] A. Steinchen, D. Gallez, A. Sanfeld, A viscoelastic approach to the hydrodynamic stability of membranes, J. Colloid Interface Sci. 85 (1982) 5–15.

[83] D.S. Dimitrov, Electric field-induced breakdown of lipid bilayer and cell membranes: a thin viscoelastic film model, J. Membr. Biol. 78 (1984) 53–60.

[84] M. Hibino, M. Shigemori, H. Itoh, K. Nagayama, K. Kinosita, Membrane conductance of an electroporated cell analyzed by sub-microsecond imaging of transmembrane potential, Biophys. J. 59 (1991) 209–220.

[85] M. Hibino, H. Itoh, K. Kinosita, Time courses of electroporation as revealed by submicrosecond imaging of transmembrane potential, Biophys. J. 64 (1993) 1789–1800.

[86] R.E. Jacobs, B.S. Hudson, H.C. Andersen, A theory of the chain melting phase transition of aqueous phospholipid dispersions, Proc. Natl. Acad. Sci. U.S.A. 72 (1975) 3993–3997.

[87] R.E. Jacobs, B.S. Hudson, H.C. Andersen, A theory of phase transitions and phase diagrams for one- and two-component phospholipid bilayers, Biochemistry 16 (1977) 4349–4359.

[88] L. Cruzeiro-Hansson, O.G. Mouritsen, Passive ion permeability of lipid membranes modelled via lipid-domain interfacial area, Biochim. Biophys. Acta 944 (1988) 63–72.

[89] L. Cruzeiro-Hansson, J.H. Ipsen, O.G. Mouritsen, Intrinsic molecules in lipid membranes change the lipid-domain interfacial area: cholesterol at domain interfaces, Biochim. Biophys. Acta 979 (1989) 166–176.

[90] J.D. Litster, Stability of lipid bilayers and red blood cell membranes, Phys. Lett. 53A (1975) 193–194.

[91] C. Taupin, M. Dvolaitzky, C. Sauterey, Osmotic pressure induced pores in phospholipid vesicles, Biochemistry 14 (1975) 4771–4775.

[92] J.C. Weaver, R.A. Mintzer, Decreased bilayer stability due to transmembrane potentials, Phys. Lett. 86A (1981) 57–59.

[93] J.N. Israelachvili, R.M. Pashley, Measurement of the hydrophobic interaction between two hydrophobic surfaces in aqueous electrolyte solutions, J. Colloid Interface Sci. 98 (1984) 500–514.

[94] A. Barnett, J.C. Weaver, Electroporation: a unified quantitative theory of reversible electrical breakdown and rupture, Bioelectrochem. Bioenerg. 25 (1991) 163–182.

[95] S.A. Freeman, M.A. Wang, J.C. Weaver, Theory of electroporation for a planar bilayer membrane: predictions of the fractional aqueous area, change in capacitance and pore-pore separation, Biophys. J. 67 (1994) 42–56.

[96] M.P. Rols, J. Teissié, Modulation of electrically induced permeabilizaiton and fusion of Chinese hamster ovary cells by osmotic pressure, Biochemistry 29 (1990) 4561–4567.

[97] M. Golzio, M.P. Mora, C. Raynaud, C. Delteil, J. Teissié, M.P. Rols, Control by osmotic pressure of voltage-induced permeabilization and gene transfer in mammalian cells, Biophys. J. 74 (1998) 3015–3022.

[98]   E. Neumann, S. Kakorin, K. Tönsing, Fundamentals of electroporative delivery of drugs and genes, Bioelectrochem. Bioenerg. 48 (1999) 3–16.

[99]   J. Teissié, M. Golzio, M.P. Rols, Mechanisms of cell membrane electropermeabilization: a minireview of our present (lack of č) knowledge, Biochim. Biophys. Acta 1724 (2005) 270–280.

[100] S. Orlowski, L.M. Mir, Cell electroporation: a new tool for biochemical and pharmacological studies, Biochim. Biophys. Acta 1154 (1993) 51–62.

[101] M.J. Jaroszeski, R. Heller, R. Gilbert, Electrochemotherapy, Electrogenetherapy and Trans-dermal Drug Delivery: Electrically Mediated Delivery of Molecules to Cells, Humana Press, Totowa, NJ, 1999.

[102] J.C. Maxwell, Treatise on Electricity and Magnetism, Oxford University Press, London, 1873.

[103] K.S. Cole, Membrane, Ions and Impulses, University of California Press, Los Angeles, 1968.

[104] K.R. Foster, H.P. Schwan, Dielectric properties of tissues, in: C. Polk, E. Postow (Eds.), Handbook of Biological Effects of Electromagnetic Fields, CRC Press, Florida, 1986, pp. 28–96.

[105] J.D. Jackson, Classical Electrodynamics, Wiley, New York, 1999.

[106] U. Zimmermann, The effect of high-intensity electric pulses on eukaryotic cell membranes, in: U. Zimmermann, G.A. Neil (Eds.), Electromanipulation of Cells, CRC press, London, 1996, pp. 1–105.

[107] E. Tekle, R.D. Astumian, P.B. Chock, Electro-permeabilization of cell membranes: effect of the resting membrane potential, Biochem. Biophys. Res. Commun. 172 (1990) 282–287.

[108] J. Teissié, M.P. Rols, An experimental evaluation of the critical potential difference inducing cell membrane electropermeabilization, Biophys. J. 65 (1993) 409–413.

[109] V.H. Pauly, H.P. Schwan, ber die Impedanz einer Suspension von kugelfrmigen Teilchen mit einer Schale, Z. Naturforsch. 14b (1959) 125–131.

[110] T. Kotnik, F. Bobanović, D. Miklavčič, Sensitivity of transmembrane voltage induced by applied electric fields: a theoretical analysis, Bioelectrochem. Bioenerg. 43 (1997) 285–291.

[111] S. Takashima, Electrical Properties of Biopolimers and Membranes, Adam Hilger, Bristol, 1989.

[112] K.H. Schoenbach, S.J. Beebe, E.S. Buescher, Intracellular effect of ultrashort electrical pulses, Bioelectromagnetics 22 (2001) 440–448.

[113] T. Kotnik, D. Miklavčič, T. Slivnik, Time course of transmembrane voltage induced by time-varying electric fields-a method for theoretical analysis and its application, Bioelectrochem. Bioenerg. 45 (1998) 3–16.

[114] R. Susil, D. Šemrov, D. Miklavčič, Electric field-induced transmembrane potential depends on cell density and organization, Electro Magnetobiol. 17 (1998) 391–399.

[115] M. Pavlin, N. Pavšelj, D. Miklavčič, Dependence of induced transmembrane potential on cell density arrangement and cell position inside a cell system, IEEE Trans. Biomed. Eng. 49 (2002) 605–612.

[116] M. Kummrow, W. Helfrich, Deformation of giant lipid vesicles by electric fields, Phys. Rew. A 44 (1991) 8356–8360.

[117] K.J. Müller, V.L. Sukhorukov, U. Zimmermann, Reversible electropermeabilization of mammalian cells by high-intensity, ultra-short pulses of submicrosecond duration, J. Membr. Biol. 184 (2001) 161–170.

[118] R.P. Joshi, Q. Hu, K.H. Schoenbach, H. P. Hjalmarson, Theoretical predictions of electro-mechanical deformation of cells subjected to high voltages for membrane electroporation, Phys. Rev. E, 65 (2002) 021913.

[119] S.I. Sukharev, V.A. Klenchin, S.M. Serov, L.V. Chernomordik, Y.A. Chizmadzhev, Electroporation and electrophoretic DNA transfer into cells. The effect of DNA interaction with electropores, Biophys. J. 63 (1992) 1320–1327.

[120] M.P. Rols, C. Delteil, M. Golzio, P. Dumond, S. Cros, J. Teissié, In vivo electrically mediated protein and gene transfer in murine melanoma, Nat. Biotechnol. 16 (1998) 168–171.

[121] S. Satkauskas, M.F. Bureau, M. Puc, A. Mahfoudi, D. Scherman, D. Miklavčič D, L.M. Mir, Mechanisms of in vivo DNA electrotransfer: respective contributions of cell electropermeabilization and DNA electrophoresis, Mol. Ther. 5 (2002) 133–140.

[122] K. Kinosita, T.Y. Tsong, Voltage-induced conductance in human erythrocyte, Biochim. Biophys. Acta 554 (1979) 479–497.

[123] I.G. Abidor, A.I. Barbul, D.V. Zhelev, P. Doinov, I.N. Bandarina, E.M. Osipova, S.I. Sukharev, Electrical properties of cell pellet and cell fusion in a centrifuge, Biochim. Biophys. Acta. 115 (1993) 207–218.

[124] I.G. Abidor, L.-H. Li, S.W. Hui, Studies of cell pellets: II. Osmotic properties, electroporation, and related phenomena: membrane interactions, Biophys. J. 67 (1994) 427–435.

[125] M. Pavlin, M. Kandušer, M. Reberšek, G. Pucihar, F.X. Hart, R. Magjarević, D. Miklavčič, Effect of cell electroporation on the conductivity of a cell suspension, Biophys. J. 88 (2005) 4378–4390.

[126] K. Schwister, B. Deuticke, Formation and properties of aqueous leaks induced in human erythrocytes by electrical breakdown 816 (1985) 332–348.

[127] B. Gabriel, J. Teissié, Fluorescence imaging in the millisecond time range of membrane electropermeabilization of single cells using a rapid ultra-low-light intensifying detection system, Eur. Biophys. J. 27 (1998) 291–298.

[128] B. Gabriel, J. Teissié, Time courses of mammalian cell electropermeabilization observed by millisecond imaging of membrane property changes during the pulse, Biophys. J. 76 (1999) 2158–2165.

[129] D. Miklavčič, D. Šemrov, H. Mekid, L.M. Mir, A validated model of in vivo electric field distribution in tissues for electrochemotherpy and for DNA electrotransfer for gene therapy, Biochim. Biophys. Acta 1519 (2000) 73–83.

[130] M. Pavlin, D. Miklavčič, Effective conductivity of a suspension of permeabilized cells: a theoretical analysis, Biophys. J. 85 (2003) 719–729.

[131] K. Kinosita, T.Y. Tsong, Voltage-induced pore formation and hemolysis of human erytrocytes, Biochim. Biophys. Acta 471 (1977) 227–242.

[132] K. Kinosita, T.Y. Tsong, Formation and resealing of pores of controlled sizes in human erythrocyte membrane, Nature 268 (1977) 438–441.

[133] A.L. Garner, N.Y. Chen, J. Yang, J. Kolb, R.J. Swanson, K.C. Loftin, S.J. Beebe, R.P. Joshi, K.H. Schoenbach, Time domain dielectric spectroscopy measurements of HL-60 cell suspensions after microsecond and nanosecond electrical pulses, IEEE Trans. Plasma Sci. 32 (2004) 2073–2084.

[134] M. Schmeer, T. Seipp, U. Pliquett, S. Kakorin, E. Neumann, Mechanism for the conductivity changes caused by membrane electroporation of CHO cell-pellets, Phys. Chem. Chem. Phys. 6 (2004) 5564–5574.

[135] R.V. Davalos, B. Rubinsky, D.M. Otten, A feasibility study for electrical impedance tomography as a means to monitor tissue electroporation for molecular medicine, IEEE Trans. Biomed. Eng. 49 (2002) 400–403.

[136] U. Pliquett, R. Elez, A. Piiper, E. Neumann, Electroporation of subcutaneous mouse tumors by rectangular and trapezium high voltage pulses, Bioelectrochemistry 62 (2004) 83–93.

[137] M. Pavlin, V. Leben, D. Miklavčič, Electroporation in dense cell suspension-Theoretical and experimental analysis of ion diffusion and cell permeabilization, Biochim. Biophys. Acta 1770 (2007) 12–23.

[138] M.P. Rols, J. Teissié, Ionic-strength modulation of electrically induced permeabilization and associates fusion of mammalian cells, Eur. J. Biochem. 179 (1989) 109–115.

[139] M.P. Rols, J. Teissié, Experimental evidence for involvement of the cytoskeleton in mammalian cell electropermeabilization, Biochim. Biophys. Acta 1111 (1992) 45–50.

[140] M.P. Rols, J. Teissié, The time course of electropermeabilization, in: M. Blank, (Ed.), Electricity and Magnetism in Biology and Medicine, San Francisco Press, San Francisco, 1993, pp. 151–154.

[141] M.P. Rols, J. Teissié, Electropermeabilization of mammalian cells to macromolecules: control by pulse duration, Biophys. J. 75 (1998) 1415–1423.

[142] T. Kotnik, G. Pucihar, M. Reberšek, L.M. Mir, D. Miklavčič, Role of pulse shape in cell membrane electropermeabilization, Biochim. Biophys. Acta 1614 (2003) 193–200.

[143] J. Teissié, C. Ramos, Correlation between electric field pulse induced long-lived perm-
      eabilization and fusogenicity in cell membranes, Biophys. J. 74 (1998) 1889–1898.
[144] I.P. Sugár, E. Neumann, Stochastic model for electric field-induced membrane pores elect-
      roporation, Biophys. Chem. 19 (1984) 211–225.
[145] D.C. Chang, T.S. Reese, Changes in membrane structure induced by electroporation as
      revealed by rapid freezing electron microscopy, Biophys. J. 58 (1990) 1–12.
[146] M. Fosnarič, V. Kralj-Iglič, K. Bohinc, A. Iglič, S. May, Stabilization of pores in lipid bilayers by
      anisotropic inclusions, J. Phys. Chem. B 107 (2003) 12519–12526.
[147] L.V. Chernomordik, S.I. Sukarev, S.V. Popov, V.F. Pastushenko, A.V. Sokirko, I.G. Abidor, Y.A.
      Chizmadzev, The electrical breakdown of cell and lipid membranes: the similarity of
      phenomenologies, Biochim. Biophys. Acta 902 (1987) 360–373.
[148] S.J. Marrink, E. Lindahl, O. Edholm, A.E. Mark, Simulation of the spontaneous aggregation of
      phospholipids into bilayers 123 (2001) 8638–8639.
[149] D.P. Tieleman, H. Leontiadou, A.E. Mark, S.J. Marrink, Simulation of pore formation in lipid
      bilayers by mechanical stress and electric fsields, J. Am. Chem. Soc. 125 (2003) 6282–6383.
[150] A. Parsegian, Energy of an ion crossing a low dielectric membrane: Solutions to four relevant
      electrostatic problems 221 (1969) 844–846.
[151] K.A. DeBruin, W. Krassowska, Modeling electroporation in a single cell. I. Effects of field
      strength and rest potential, Biophys. J. 77 (1999) 1213–1223.
[152] K.A. DeBruin, W. Krassowska, Modeling electroporation in a single cell. II. Effects of ionic
      concentrations, Biophys. J. 77 (1999) 1225–1233.